

Double-crossing mode conversion in nonuniform media

A. J. Brizard, J. J. Morehead, and A. N. Kaufman
Lawrence Berkeley National Laboratory, Berkeley, California 94720

E. R. Tracy
Department of Physics, College of William and Mary, Williamsburg, Virginia 23185

(Received 21 August 1997; accepted 8 September 1997)

A new type of mode conversion between two linear waves in a nonuniform medium is investigated. Single-crossing conversion occurs when a ray of one wave crosses *transversely* the dispersion manifold of another wave. *Double-crossing* mode conversion theory describes when the ray punctures the dispersion manifold twice due to ray *curvature*. To study this new process, a one dimensionally nonuniform background medium is considered, which gives rise to four scenarios. These scenarios are distinguished on the basis of whether the two waves have equal or opposite energy signs, and whether they are copropagating or counterpropagating. Using *modular-eikonal* theory (suitable for multiple crossings), each scenario is first studied analytically by constructing an S-matrix relation between the *outgoing* and *incoming* asymptotic wave amplitudes. The analytical results are then compared with numerical results and excellent agreement is found. © 1998 American Institute of Physics. [S1070-664X(98)04401-2]

I. INTRODUCTION

A. The ray picture

The standard treatment of mode conversion (based on ray phase-space mode conversion theory)^{1,2} begins with the concept of a ray orbit of a linear wave supported by a time-independent background medium. A ray evolves according to the Hamilton equations: $\dot{\mathbf{x}}^j = \partial \omega_j(\mathbf{x}, \mathbf{k}) / \partial \mathbf{k}$, $\dot{\mathbf{k}}^j = -\partial \omega_j(\mathbf{x}, \mathbf{k}) / \partial \mathbf{x}$, where j is a wave label (the background medium typically can support more than one wave type at a time), \mathbf{k} and \mathbf{x} are the wave vector and spatial coordinates of a point in ray phase space (the dot represents a time derivative), respectively, and the *Hamiltonian* $\omega_j(\mathbf{k}, \mathbf{x})$ is a root of the dispersion function $D_j(\mathbf{k}, \mathbf{x}; \omega)$. We note that all ray orbits of wave j lie entirely on the dispersion manifold $\mathcal{M}_j \equiv \{\mathbf{x}, \mathbf{k} | D_j(\mathbf{k}, \mathbf{x}; \omega) = 0\}$ and that the Hamiltonian equations can also be written as

$$\dot{\mathbf{x}}^j \equiv -(\partial_{\mathbf{k}} D_j) / (\partial_{\omega} D_j), \quad \dot{\mathbf{k}}^j \equiv (\partial_{\mathbf{x}} D_j) / (\partial_{\omega} D_j). \quad (1)$$

We also note that the sign of the wave energy for wave j is given by the sign of $\partial_{\omega} D_j$, and that a ray orbit possesses *curvature* when its tangent vector $(\dot{\mathbf{x}}^j, \dot{\mathbf{k}}^j)$ is not a constant, i.e., $(\ddot{\mathbf{x}}^j, \ddot{\mathbf{k}}^j) \neq 0$.

Mode conversion theory³ typically describes the situation [Fig. 1(a)] in which an *incident* ray of one wave type (labeled a) crosses the dispersion manifold of another wave type (labeled b). At the crossing, the two waves interact resonantly (i.e., their frequencies and wave vectors match), and, through mode conversion, transfer of wave action (as well as energy and momentum) from the incident wave a creates a *converted* ray orbit for wave b and a *transmitted* ray orbit for wave a , both of which eventually leave the conversion region [Fig. 1(b)]. Generally, the crossing occurs *transversely* and, in the local approximation, the dispersion manifold for wave b (denoted \mathcal{M}_b) may be approximated by its tangent plane (at the crossing point), and the incident ray orbit (denoted \mathcal{R}_a) may be approximated by a straight line.

When the crossing of the incident ray \mathcal{R}_a with the dispersion manifold \mathcal{M}_b is *near-tangential* [Fig. 1(c)], however, the respective *curvatures* of \mathcal{R}_a and \mathcal{M}_b become important. In particular, a large curvature in either the incoming ray \mathcal{R}_a or the dispersion manifold \mathcal{M}_b makes a “nearby” second crossing point possible.

The primary goal of this work is to investigate the effect of curvature on linear mode conversion; in particular, the situation in which double crossing occurs is studied analytically and numerically. In what follows, we consider double-crossing mode conversion in a one-dimensional background medium, with gradients directed along the x axis. In this case, the dispersion manifold $\mathcal{M}_b = \{x, k_x | D_b(x, k_x) = 0\}$ for wave b is a curve $x_b(k_x)$, or $k_x^b(x)$, in the (x, k_x) plane.

B. Double crossing of parabolic rays

To study ray-curvature effects in one-dimensional mode conversion, we consider a simple model [see (6)] wherein double-crossing mode conversion occurs in the neighborhood of two *caustics*, i.e., the *uncoupled* rays for each wave are *parabolas* [see Fig. 2(a)] of the form

$$x_j(k_x) = x_{j0} + \beta_j k_x^2. \quad (2)$$

Here $x_{j0} \equiv x_j(k_x = 0)$ represents the location of a caustic for wave j [i.e., $dk_x^j(x)/dx$ becomes infinite at $x = x_{j0}$] and $\beta_j \equiv dx_j(k_x)/dk_x^2$ is the constant (signed) ray *curvature*. Within this model, two intersecting (uncoupled) parabolic rays [see Fig. 2(a)] cross *twice* at $(x^c, \pm k_x^c)$, where $(k_x^c)^2 \equiv (x_{a0} - x_{b0}) / (\beta_b - \beta_a)$ and $x^c \equiv x_{j0} + \beta_j (k_x^c)^2$. To satisfy the crossing condition $(k_x^c)^2 > 0$, the caustic separation Δx and the ray-curvature difference $\Delta \beta$ are defined,

$$\Delta x \equiv x_{a0} - x_{b0} > 0 \quad \text{and} \quad \Delta \beta \equiv \beta_b - \beta_a > 0, \quad (3)$$

so that $k_x^c \equiv (\Delta x / \Delta \beta)^{1/2}$. [The sign conventions adopted above are chosen to agree with Fig. 2(a), where $\beta_a < \beta_b < 0$

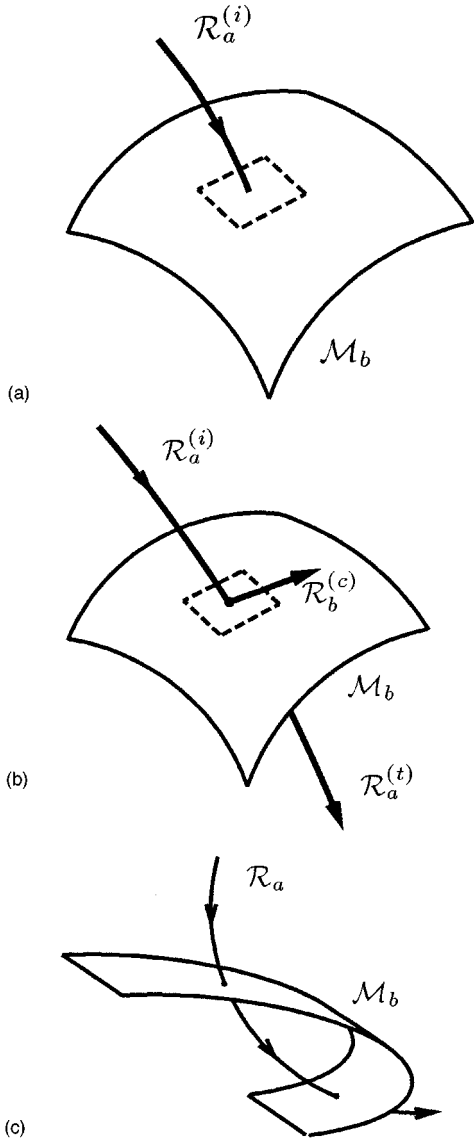


FIG. 1. (a) An incident ray $\mathcal{R}_a^{(i)}$ of type a crosses transversely the dispersion manifold \mathcal{M}_b of wave type b ; (b) mode conversion occurs when some of the action from $\mathcal{R}_a^{(i)}$ gets converted to a ray $\mathcal{R}_b^{(c)}$ of type b (which stays on the dispersion manifold \mathcal{M}_b), and the remaining action leaves \mathcal{M}_b as the transmitted ray $\mathcal{R}_a^{(t)}$; (c) when the crossing takes place near-tangentially, ray curvature becomes important and makes a nearby second crossing possible.

and $x_{a0} > x_{b0}$; the case $\Delta x < 0$ corresponds to *noncrossing* parabolas and, because of its mathematical complexity, is beyond the scope of this work.]

C. Coupled wave equations

We now derive a set of coupled linear wave equations for waves a and b represented, respectively, by the wave fields $\Psi_a(k_x)$ and $\Psi_b(k_x)$. Here, since the x representation for (2) is *singular*, i.e., $k_x^j(x) = \pm[(x - x_{j0})/\beta_j]^{1/2}$ has a (caustic) singularity at $x = x_{j0}$, the k_x representation for the wave fields (where $x \rightarrow \hat{x} \equiv id/dk_x$) is adopted throughout this paper.

The variational principle used to derive our coupled wave equations is based on the action integral,³ \mathcal{A}

$= \int \Psi^\dagger(k_x) \cdot D(\hat{x}, k_x) \cdot \Psi(k_x) dk_x$, where $\Psi(k_x)$ is a multi-component field and D is a Hermitian differential operator through its dependence on \hat{x} . Since we are interested in studying mode conversion between waves of types a and b , we introduce the projection $\Psi \equiv \sum_{j=a,b} \hat{e}_j \Psi_j$, where Ψ_j and \hat{e}_j are the amplitude and polarization of wave j . By defining the dispersion function for wave j as $D_j(\hat{x}, k_x) \equiv \mathbf{e}_j^* \cdot D(\hat{x}, k_x) \cdot \mathbf{e}_j$, and the coupling coefficient between waves a and b as $\eta \equiv \mathbf{e}_a^* \cdot D(\hat{x}, k_x) \cdot \mathbf{e}_b$, the action integral becomes

$$\mathcal{A} = \int dk_x \left(\sum_{j=a,b} \Psi_j^*(k_x) D_j(\hat{x}, k_x) \Psi_j(k_x) + 2 \operatorname{Re}[\Psi_a^*(k_x) \eta \Psi_b(k_x)] \right), \quad (4)$$

where η is evaluated at a mode-conversion point [where $\Psi_j(k_x)$ displays rapid k_x dependence] and the constant η is assumed to be the same at both conversion points. The variational principle $\delta \mathcal{A} = 0$ requires that \mathcal{A} be stationary with respect to arbitrary variations in Ψ_a^* and Ψ_b^* , which yields a set of coupled wave equations for Ψ_a and Ψ_b , written in matrix form¹ as

$$\begin{pmatrix} D_a(\hat{x}, k_x) & \eta \\ \eta^* & D_b(\hat{x}, k_x) \end{pmatrix} \begin{pmatrix} \Psi_a(k_x) \\ \Psi_b(k_x) \end{pmatrix} = 0. \quad (5)$$

In (4) and (5), additional dependences on k_y and k_z and the wave frequency ω (common to both waves) are not displayed for brevity (note that, for a time-independent background medium that is uniform in the spatial coordinates y and z , the variables ω , k_y , and k_z are constant along a ray).

In order to study double-crossing mode conversion near two caustics, each dispersion function $D_j(x, k_x)$ in (5), near its caustic (at $x = x_{j0}$ and $k_x = 0$), has the form

$$D_j(x, k_x) = (\partial D_j / \partial x)_0 (x - x_{j0}) + (\partial D_j / \partial k_x^2)_0 k_x^2 \equiv (\partial_x D_j)_0 (x - x_{j0} - \beta_j k_x^2), \quad (6)$$

where $(\partial D_j / \partial x)_0$ and $(\partial D_j / \partial k_x^2)_0$ are both evaluated at the caustic, and the ray curvature for wave j is defined $\beta_j \equiv -(\partial_{k_x^2} D_j)_0 / (\partial_x D_j)_0$ [see (2)]. Note that, in general, both x_{j0} and β_j are functions of k_y , k_z , and ω . Important examples of dispersion functions of the form (6) are found in the theory of linear waves in nonuniform magnetized plasmas (e.g., linear drift waves). Generically, such waves have dispersion functions $D(x, k_\perp; k_y, k_z, \omega)$, where the background plasma is nonuniform in the x direction, the background magnetic field is aligned along the z axis, and the k_x dependence enters only through $k_\perp^2 \equiv k_x^2 + k_y^2$. Taylor expansion of $D(x, k_\perp)$ in the neighborhood of a caustic (at $k_x = 0$) yields (6).

D. Wave-action conservation law

The variational principle (4) allows the derivation of conservation laws through the Noether method (i.e., for each continuous symmetry of the Lagrangian, there exists a conserved quantity). In particular, the Lagrangian in (4) is sym-

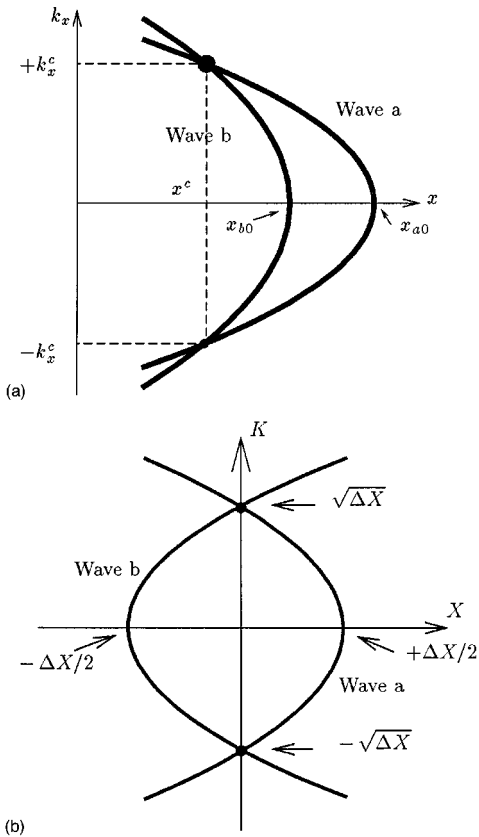


FIG. 2. (a) Double-crossing mode conversion near two caustics (here, the curvatures β_a and β_b are both negative), parametrized by the caustic separation $\Delta x = x_{a0} - x_{b0}$, the curvature difference $\Delta\beta = \beta_b - \beta_a$, and the wave-coupling strength η ; (b) symmetric double-crossing mode conversion parametrized by only the dimensionless parameters ΔX and $\bar{\eta}$, defined in (13).

metric with respect to phase shifts in the wave functions,⁴ and the corresponding conservation law is the wave-action conservation law:

$$\sum_{j=a,b} dJ_j(k_x)/dk_x = 0, \quad (7)$$

where

$$\begin{aligned} J_j(k_x) &\equiv \Psi_j^*(k_x) \frac{\partial D_j}{\partial x}(\hat{x}, k_x) \Psi_j(k_x) \\ &= (\partial D_j / \partial x)_0 |\Psi_j(k_x)|^2 \end{aligned} \quad (8)$$

denotes the wave-action density flux (in k_x space) for wave j . The last expression in (8) follows from (6) in the local approximation. When (7) is integrated over k_x from “ $-\infty$ ” to “ $+\infty$ ” (i.e., sufficiently far from the double-crossing mode conversion region), we obtain

$$J_a(+\infty) + J_b(+\infty) = J_a(-\infty) + J_b(-\infty). \quad (9)$$

By defining $\Delta J_j \equiv J_j(+\infty) - J_j(-\infty)$ as the change in wave-action density flux for wave j , Eq. (9) can be rewritten as $\Delta J_a = -\Delta J_b$; this means that, for linear mode conversion involving waves a and b , any change in wave-action density flux for wave a is compensated by an equal but opposite change in wave-action density flux for wave b . The conser-

vation law (9) provides us with a powerful tool in interpreting our analytical results and in comparing them with numerical results.

E. Organization

The remainder of this paper is organized as follows. In Sec. II, we present the coupled-wave equations (in dimensionless form) associated with four distinct scenarios for double-crossing mode conversion in a one dimensionally nonuniform medium. The four scenarios are distinguished on the basis of whether the two waves have equal or opposite energy signs, and whether they are copropagating or counterpropagating in k_x . The analysis is greatly facilitated by the existence of the conservation law (9), which allows us to relate incoming and outgoing asymptotic wave amplitudes through a global \mathbf{S} matrix.

In Sec. III, we introduce the modular-eikonal approach used to obtain explicit expressions for the global \mathbf{S} matrix for each scenario. After discussing its validity, we summarize our analytical results and present a comparison between these results and numerical results obtained by integrating the coupled-wave equations themselves. The results of the modular-eikonal approach are then shown to be in excellent agreement with the numerical results. In Secs. IV and V, as well as Appendices A–D, we present the technical details of the derivation of our results. Finally, in Sec. VI, we review our results and discuss the assumptions used in the modular-eikonal approach and its extensions.

II. MODE CONVERSION IN A ONE DIMENSIONALLY NONUNIFORM MEDIUM

A. Four scenarios

Our analysis of the coupled equations (5), with the dispersion functions (6), is based on the relative signs of $(\partial_x D_a)_0$ and $(\partial_x D_b)_0$. From (1), we note that the sign of $(\partial_x D_j)_0$, denoted ϵ_j , is the product of the sign of $(\partial_\omega D_j)_0$, which determines the sign of the *wave energy* for wave j , and the sign of $(\dot{k}_x^j)_0$, which determines its direction of *propagation* along the k_x axis:

$$\epsilon_j \equiv \text{sign}[(\partial_x D_j)_0] \equiv \text{sign}[(\partial_\omega D_j)_0] \text{sign}[(\dot{k}_x^j)_0]. \quad (10)$$

In what follows, we distinguish between four different *scenarios*, depending on whether the signs of $(\partial_\omega D_a)_0$ and $(\partial_\omega D_b)_0$ are equal or opposite (i.e., whether the energy signs of waves a and b are equal or opposite), and whether the signs of \dot{k}_{x0}^a and \dot{k}_{x0}^b are equal or opposite (i.e., whether waves a and b are co-propagating or counterpropagating). These scenarios are summarized and labeled in Table I.

For definiteness, the values of ϵ_a and ϵ_b shown above are used throughout this work. Hence, in all four scenarios [shown in Figs. 3(a)–3(d)], wave a is always viewed as a positive-energy wave propagating upward in k_x . Wave b , on the other hand, has the following characteristics: in scenario I, it is a copropagating positive-energy wave, i.e., it is also propagating upward in k_x ; in scenario II, it is a counterpropagating positive-energy wave; in scenario III, it is a copropagating negative-energy wave; and finally, in scenario IV, it is a counterpropagating negative-energy wave.⁵

TABLE I. Double-crossing mode conversion scenarios.

Scenario	Wave-energy signs	Propagation directions	$\epsilon_j \equiv \text{sign}[(\partial_x D_j)_0]$
I	Equal	Copropagation	$\epsilon_a = +1 = \epsilon_b$
II	Equal	Counterpropagation	$\epsilon_a = +1 = -\epsilon_b$
III	Opposite	Copropagation	$\epsilon_a = +1 = -\epsilon_b$
IV	Opposite	Counterpropagation	$\epsilon_a = +1 = \epsilon_b$

B. Dimensionless equations

In the process of solving the coupled equations (5)–(6), only the curvature difference $\Delta\beta$ and the caustic separation Δx enter into the analysis of the double-crossing mode conversion problem. First, we symmetrize the double-crossing mode conversion process by performing the transformation

$$\Psi_j(k_x) \equiv \bar{\Psi}_j(k_x) \exp\left(-i \int x_0(k_x) dk_x\right), \quad (11)$$

where $x_0(k_x) \equiv (1/2)[(x_{a0} + x_{b0}) + (\beta_a + \beta_b)k_x^2]$, so that, using (6), $D_j(\hat{x}, k_x)\Psi_j(k_x)$ becomes

$$\begin{aligned} D_j(\hat{x}, k_x)\Psi_j(k_x) &\equiv (\partial_x D_j)_0 [\hat{x} - x_j(k_x)] \bar{\Psi}_j(k_x) \\ &\quad \times \exp\left(-i \int x_0(k_x) dk_x\right) \\ &= (\partial_x D_j)_0 \exp\left(-i \int x_0(k_x) dk_x\right) \\ &\quad \times [\hat{x} - \bar{x}_j(k_x)] \bar{\Psi}_j(k_x), \end{aligned} \quad (12a)$$

where $\bar{x}_j(k_x) \equiv x_j(k_x) - x_0(k_x)$. Combining these results, the coupled equations (5) become

$$\begin{aligned} (\partial_x D_a)_0 [\hat{x} - \bar{x}_a(k_x)] \bar{\Psi}_a(k_x) + \eta \bar{\Psi}_b(k_x) &= 0, \\ \eta^* \bar{\Psi}_a(k_x) + (\partial_x D_b)_0 [\hat{x} - \bar{x}_b(k_x)] \bar{\Psi}_b(k_x) &= 0, \end{aligned} \quad (12b)$$

where $\bar{x}_a(k_x) = -\bar{x}_b(k_x) \equiv (1/2)(\Delta x - \Delta\beta k_x^2)$. Next, the curvature difference $\Delta\beta$ can be used to introduce the *dimensionless* (canonically conjugate) variables (X, K) :

$$X \equiv (\Delta\beta)^{-1/3} x, \quad K \equiv (\Delta\beta)^{1/3} k_x, \quad (13a)$$

and the *dimensionless* coupling strength and caustic separation:

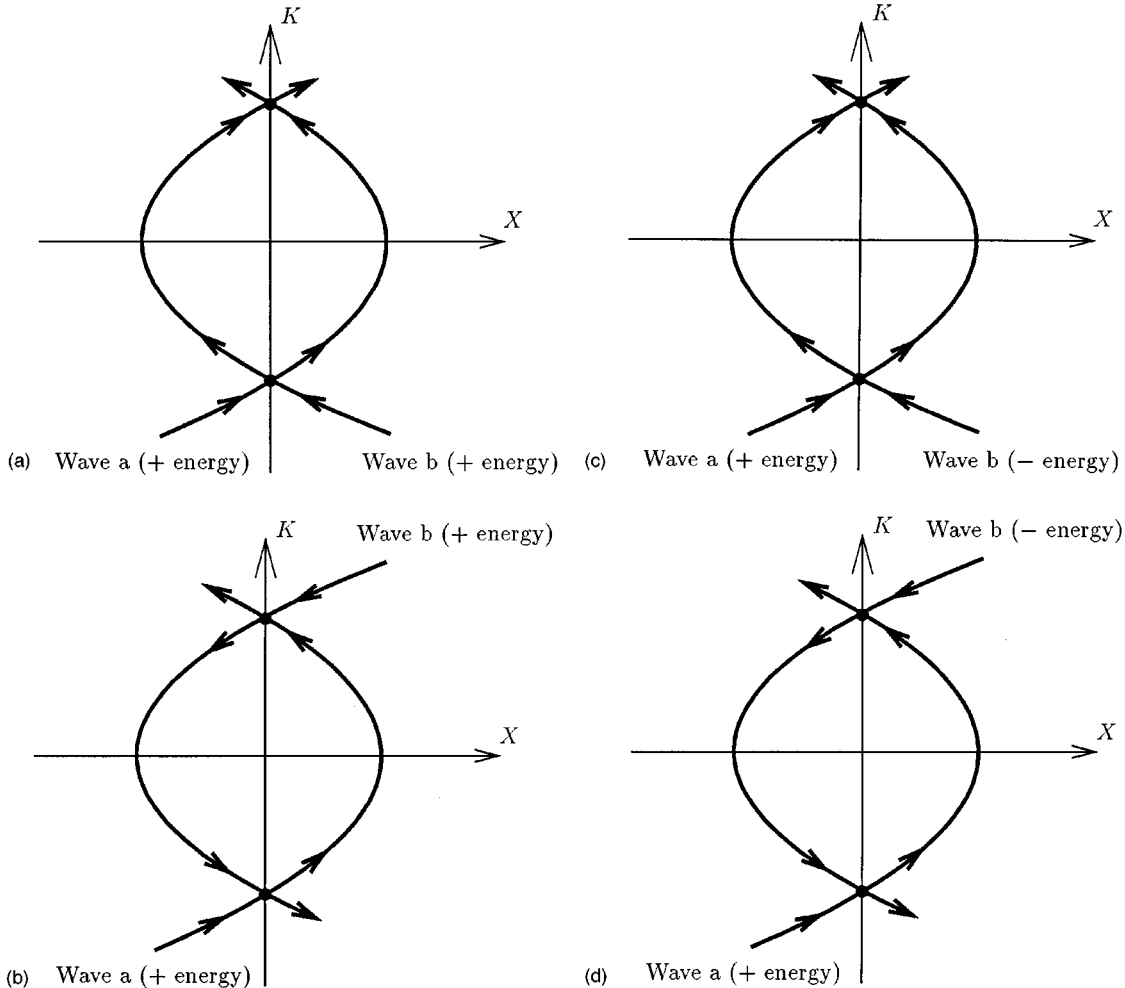


FIG. 3. Double-crossing mode-conversion scenarios I–IV, with arrows showing the direction of wave packet propagation. (a) Scenario I: two copropagating waves of equal energy signs; (b) scenario II: two counterpropagating waves of equal energy signs; (c) scenario III: two copropagating waves of opposite energy signs; (d) scenario IV: two counterpropagating waves of opposite energy signs.

$$\bar{\eta} \equiv (\Delta\beta)^{-1/3} \left(\frac{\eta}{|(\partial_x D_a)_0 (\partial_x D_b)_0|^{1/2}} \right) \quad \text{and}$$

$$\Delta X = (\Delta\beta)^{-1/3} \Delta x. \quad (13b)$$

Hence, from the original (dimensional) parameter list $(\eta, \Delta x, \Delta\beta)$, only the two dimensionless parameters $(\bar{\eta}, \Delta X)$ remain.

As suggested by the expression (8) for the wave-action density flux, we introduce the wave-action-flux *amplitude* for wave j , denoted ψ_j :

$$\psi_j(k_x) \equiv |(\partial_x D_j)_0|^{1/2} \bar{\Psi}_j(K). \quad (14)$$

When (13a), (13b), and (14) are substituted into (12b) (and keeping in mind that X becomes $\hat{X} = id/dK$ in the K representation), it becomes

$$\begin{pmatrix} \mathcal{D}_a(\hat{X}, K) & \bar{\eta} \\ \bar{\eta}^* & \mathcal{D}_b(\hat{X}, K) \end{pmatrix} \begin{pmatrix} \psi_a(K) \\ \psi_b(K) \end{pmatrix} = 0, \quad (15)$$

where constant coefficients have been eliminated from each row and the dimensionless dispersion function for wave j is $\mathcal{D}_j(X, K) \equiv \epsilon_j [X \mp (\Delta X - K^2)/2]$, where the upper (lower) signs refer to wave a (wave b). In this symmetric representation of double-crossing mode conversion [see Fig. 2(b)], the two uncoupled rays cross at crossing points with dimensionless coordinates $X=0, K = \pm \sqrt{\Delta X}$.

From (8), (11), and (14), the wave-action density flux for wave j is now simply expressed in terms of ψ_j as $J_j(K) = \epsilon_j |\psi_j(K)|^2$, so that the wave-action conservation law (9) becomes

$$|\psi_a(+\infty)|^2 + \epsilon |\psi_b(+\infty)|^2 = |\psi_a(-\infty)|^2 + \epsilon |\psi_b(-\infty)|^2, \quad (16)$$

where $\epsilon \equiv \epsilon_a \epsilon_b = +1$ for scenarios I and IV, while $\epsilon = -1$ for scenarios II and III. To make use of this conservation law, we thus need to investigate the asymptotic behavior of the wave functions $\psi_a(K)$ and $\psi_b(K)$ as $K \rightarrow \pm\infty$.

C. Global asymptotic analysis

Before considering the global asymptotic behaviors of $\psi_a(K)$ and $\psi_b(K)$ (at $K = \pm\infty$), we investigate the mode-conversion regions (near $K = \pm\sqrt{\Delta X}$). Near each of these two points, the *ray* picture (based on the validity of the eikonal representation) breaks down. To present a more accurate picture, we need instead the *dispersion curves* of the dispersion matrix in (15), defined by the vanishing of its determinant, $\mathcal{D}_a(X, K)\mathcal{D}_b(X, K) - |\bar{\eta}|^2$. Using (15), the two dispersion curves are $X^2(K) = (\Delta X - K^2)^2/4 + \epsilon |\bar{\eta}|^2$, where $\epsilon = +1$ for scenarios I and IV, and $\epsilon = -1$ for scenarios II and III. These two dispersion curves are sketched in Figs. 4(a) and 4(b), respectively; the double-arrow notation is used to indicate the direction of the wave-energy flux (in the absence of wave coupling), represented by the equations $dX_j/ds = -\partial_K \mathcal{D}_j$ and $dK_j/ds = \partial_X \mathcal{D}_j$, where s is an orbit parameter. We note that, for a positive-energy wave, its energy flux flows in the same direction as its wave packet [given by (1)], while for a negative-energy wave, its energy flux flows in the opposite direction. Hence, although waves a and b are counterpropagating waves of opposite wave-

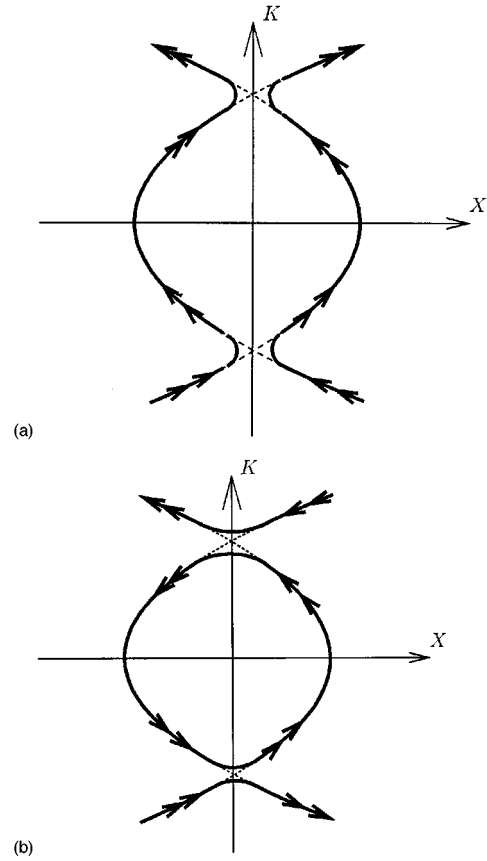


FIG. 4. Dispersion curves for (a) scenarios I and IV, and (b) scenarios II and III, with the double-arrow notation showing the direction of energy-flux propagation.

energy signs in scenario IV, their energy fluxes flow in the same direction and Fig. 4(a) applies to both scenarios I and IV; similar remarks apply to scenarios II and III.

Each dispersion curve in Figs. 4(a) and 4(b) can be divided into five regions. First, there are three regions in which the eikonal representation is valid. These three *eikonal* regions are labeled, respectively, the *upper* (or $\alpha = +$) region for $K \rightarrow +\infty$; the *intermediate* (or $\alpha = 0$) region for $|K| \rightarrow 0$; and the *lower* (or $\alpha = -$) region for $K \rightarrow -\infty$. Next, there are two *mode-coupling* regions labeled *top* (for $K \approx +\sqrt{\Delta X}$) and *bottom* (for $K \approx -\sqrt{\Delta X}$) in which the eikonal representation breaks down. Note that, in Figs. 4(a) and 4(b), a dispersion curve (far from the mode-coupling region) asymptotically approaches one of the uncoupled rays (dashed lines). Solutions of (15) in the three eikonal regions are called the *outer* solutions while those in the two mode-conversion regions are called the *inner* solutions; they are analyzed in detail in Sec. IV.

In the eikonal regions $\alpha = (-, 0, +)$, the wave fields have the asymptotic eikonal form [see (A18)]

$$\psi_j^\alpha(K) \rightarrow e^{-iS_j(K)} Z_j^\alpha, \quad (17a)$$

where the eikonal *phases* $S_j(K)$ are real valued while the eikonal (constant) *amplitudes* $Z_j^\alpha = (Z_j^+, Z_j^0, Z_j^-)$ are complex valued (see Appendix A for details). Previous work on *multiple-crossing* mode conversion⁶ has shown that, in order for the modular-eikonal method (see the next section) to be

TABLE II. Incoming and outgoing asymptotic amplitudes.

Scenario	Incoming amplitudes	Outgoing amplitudes
I	(Z_a^-, Z_b^-)	(Z_a^+, Z_b^+)
II	(Z_a^-, Z_b^+)	(Z_a^+, Z_b^-)
III	(Z_a^+, Z_b^-)	(Z_a^-, Z_b^+)
IV	(Z_a^+, Z_b^+)	(Z_a^-, Z_b^-)

successful in comparing its analytical results with numerical solutions of coupled wave equations, the eikonal phases must retain lowest-order wave-coupling corrections. In Appendix A, the expressions for the eikonal phases, including wave-coupling corrections, are found to be $S_a(K) = -S_b(K) \equiv S(K)$, with

$$S(K) \equiv \frac{1}{2} K \Delta X - \frac{1}{6} K^3 + \frac{\epsilon |\bar{\eta}|^2}{2\sqrt{\Delta X}} \ln \left(\frac{|K + \sqrt{\Delta X}|}{|K - \sqrt{\Delta X}|} \right). \quad (17b)$$

It is in the wave-coupling correction term that the *modular-eikonal* wave theory differs from the *standard* eikonal wave theory (which ignores this correction).

D. Conservation laws and S-matrix relations

Substituting $|\psi(\pm\infty)|^2 = |Z_j^\pm|^2$, from (17a), into the wave-action conservation law (16), we obtain

$$|Z_a^+|^2 + \epsilon |Z_b^+|^2 = |Z_a^-|^2 + \epsilon |Z_b^-|^2. \quad (18)$$

This conservation law can be written in a suggestive fashion if we introduce the two-component vectors $\mathbf{Z} \equiv (Z_a, Z_b)$ and the norm $\|\mathbf{Z}\|_\kappa^2 \equiv |Z_a|^2 + \kappa \epsilon |Z_b|^2$, where $\kappa = +1$ refers to *copropagating* waves (i.e., both waves are incoming either at $K = -\infty$ or $+\infty$) while $\kappa = -1$ refers to *counterpropagating waves* (i.e., one wave is incoming at $K = -\infty$ and the other at $K = +\infty$).

To proceed with the analysis of the four scenarios defined in Table I, we need to identify the incoming waves and the outgoing waves. In Table II, we list the incoming and outgoing asymptotic amplitudes used for each scenario.

Hence, for copropagating waves (i.e., scenarios I and III), the wave-action conservation law (18) is written as

$$\|\mathbf{Z}^{\text{out}}\|_+^2 \equiv |Z_a^+|^2 + \epsilon |Z_b^+|^2 = |Z_a^-|^2 + \epsilon |Z_b^-|^2 \equiv \|\mathbf{Z}^{\text{in}}\|_+^2, \quad (19a)$$

while for counter-propagating waves (i.e., scenarios II and IV), it is written as

$$\|\mathbf{Z}^{\text{out}}\|_-^2 \equiv |Z_a^+|^2 - \epsilon |Z_b^-|^2 = |Z_a^-|^2 - \epsilon |Z_b^+|^2 \equiv \|\mathbf{Z}^{\text{in}}\|_-^2. \quad (19b)$$

Mode conversion is therefore a process that transforms the incoming asymptotic amplitudes \mathbf{Z}^{in} into the outgoing asymptotic amplitudes \mathbf{Z}^{out} while conserving the norm $\|\cdot\|_\kappa$.

Thus, we look for a matrix (with unit determinant), denoted \mathbf{S}_κ , which relates the initial and final asymptotic states in the following way:

$$\mathbf{Z}^{\text{out}} = \mathbf{S}_\kappa \cdot \mathbf{Z}^{\text{in}}. \quad (20a)$$

In Appendix B, it is shown that, in order to satisfy the conservation laws (19a) and (19b), the \mathbf{S} matrix of (20a) must have the form

$$\mathbf{S}_\kappa \equiv \begin{pmatrix} \mathcal{S}_{aa} & \mathcal{S}_{ab} \\ -\kappa \epsilon \mathcal{S}_{ab}^* & \mathcal{S}_{aa}^* \end{pmatrix}, \quad (20b)$$

where \mathcal{S}_{aa} and \mathcal{S}_{ab} are complex-valued coefficients that satisfy

$$|\mathcal{S}_{aa}|^2 + \kappa \epsilon |\mathcal{S}_{ab}|^2 = 1. \quad (20c)$$

We find that each scenario has different expressions for \mathcal{S}_{aa} and \mathcal{S}_{ab} , although exact relations exist between the coefficients for scenarios I and IV [(30a)], and the coefficients for scenarios II and III [(30b)]. We also note that the matrix (20b) is unitary only when $\kappa \epsilon = +1$ (i.e., waves with equal energy signs); for the case $\kappa \epsilon = -1$ (i.e., waves with opposite energy signs), see Appendix B. We now provide physical interpretations for \mathcal{S}_{aa} and \mathcal{S}_{ab} .

When wave a alone is incoming (i.e., $Z_a^{\text{in}} \neq 0$ and $Z_b^{\text{in}} = 0$), (20a) and (20b) yields $Z_a^{\text{out}} = \mathcal{S}_{aa} Z_a^{\text{in}}$ and $Z_b^{\text{out}} = -\kappa \epsilon \mathcal{S}_{ab}^* Z_a^{\text{in}}$. From these relations, we introduce *global* transmission and conversion coefficients: the global transmission coefficient for double-crossing (D) mode conversion is defined as

$$T_D \equiv |Z_a^{\text{out}}|^2 / |Z_a^{\text{in}}|^2 = |\mathcal{S}_{aa}|^2; \quad (21a)$$

the global conversion coefficient for double-crossing mode conversion is defined as

$$C_D \equiv \kappa \epsilon |Z_b^{\text{out}}|^2 / |Z_a^{\text{in}}|^2 = \kappa \epsilon |\mathcal{S}_{ab}|^2, \quad (21b)$$

so that the wave-action conservation law (20c) becomes

$$T_D + C_D = 1. \quad (21c)$$

Hence, for each unit of incoming wave energy of wave a present before mode conversion, T_D units of wave energy of wave a and C_D units of wave energy of wave b appear after mode conversion.

The choice $\kappa \epsilon \equiv \text{sign}[(\partial_\omega D_a \partial_\omega D_b)_0]$ used in (21b) is consistent with the fact that for mode conversion between waves of opposite energy signs (either copropagating or counterpropagating), i.e., $\kappa \epsilon = -1$, we must have $C_D < 0$, since the energy sign does change at conversion⁷ and, consequently, $T_D > 1$ according to (21c).

III. SUMMARY OF THE MODULAR-EIKONAL APPROACH

A. Introduction

The modular-eikonal method is used to study multiple-crossing mode conversion problems⁶ and provides an algorithm for breaking up the *global* problem of relating the incoming amplitudes $\mathbf{Z}^{\text{in}} = (Z_a^{\text{in}}, Z_b^{\text{in}})$ to the outgoing amplitudes $\mathbf{Z}^{\text{out}} = (Z_a^{\text{out}}, Z_b^{\text{out}})$, by introducing an intermediate asymptotic state $\mathbf{Z}^0 = (Z_a^0, Z_b^0)$ in the eikonal region $K \rightarrow 0$. In this section, we assume (for simplicity) that waves a and b are both incoming from $K = -\infty$ (i.e., $\mathbf{Z}^{\text{in}} \equiv \mathbf{Z}^-$), and are outgoing at $K = +\infty$ (i.e., $\mathbf{Z}^{\text{out}} \equiv \mathbf{Z}^+$).

Figure 5 illustrates the various steps involved in the modular-eikonal approach for finding the outgoing wave am-

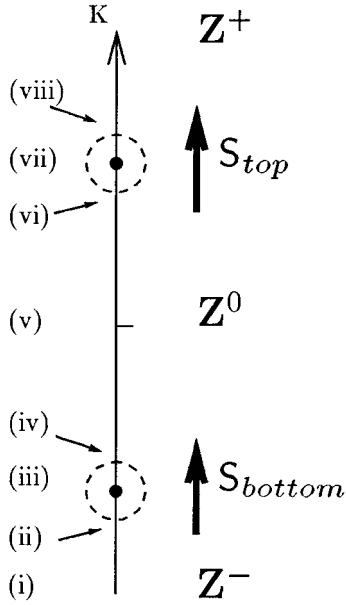


FIG. 5. Steps involved in the modular-eikonal approach (see the text for a description).

plitudes once the incoming wave amplitudes are known. In step (i), the incoming outer solutions (with asymptotic amplitudes \mathbf{Z}^-) are defined in the lower asymptotic region ($K \rightarrow -\infty$). Asymptotic matching between inner and outer solutions is performed in steps (ii) and (iv) for the bottom mode-conversion region, and steps (vi) and (viii) for the top mode-conversion region. In steps (iii) and (vii), we use the results of the analysis in the bottom and top mode-conversion regions to relate incoming and outgoing inner solutions. In step (v), the intermediate asymptotic amplitude \mathbf{Z}^0 is expressed in terms of \mathbf{Z}^- with the help of the bottom single-crossing \mathbf{S} matrix $\mathbf{S}_{\text{bottom}}$:

$$\mathbf{Z}^0 \equiv \mathbf{S}_{\text{bottom}} \cdot \mathbf{Z}^- . \quad (22a)$$

The \mathbf{S} -matrix relation between the incoming asymptotic amplitudes \mathbf{Z}^0 and the outgoing asymptotic amplitudes \mathbf{Z}^+ at the top mode conversion,

$$\mathbf{Z}^+ \equiv \mathbf{S}_{\text{top}} \cdot \mathbf{Z}^0 , \quad (22b)$$

involves the top single-crossing \mathbf{S} matrix \mathbf{S}_{top} .

By eliminating the intermediate asymptotic amplitudes \mathbf{Z}^0 [i.e., by substituting (22a) into (22b)], a *global* double-crossing \mathbf{S} matrix (denoted $\mathbf{S}_{\text{global}}$), which relates the outgoing eikonal amplitudes \mathbf{Z}^+ to the incoming eikonal amplitudes \mathbf{Z}^- , is defined as

$$\mathbf{Z}^+ = \mathbf{S}_{\text{top}} \cdot (\mathbf{S}_{\text{bottom}} \cdot \mathbf{Z}^-) \equiv \mathbf{S}_{\text{global}} \cdot \mathbf{Z}^- . \quad (23)$$

Thus, according to the modular-eikonal approach, the calculation of the global \mathbf{S} matrix for double-crossing mode conversion is done by calculating the \mathbf{S} matrices for both (top and bottom) single-crossing mode conversions.

B. Validity of the modular approach

The principal assumption behind the modular approach is that the *intermediate* eikonal region is large enough for the wave fields to enter the eikonal regime. In Appendix A [(A11)], we show that the eikonal representation is valid in the intermediate region when

$$|\Delta X| \gg |\bar{\eta}| . \quad (24)$$

For $|\bar{\eta}|$ of order unity, this condition becomes $|\Delta X| \gg 1$.

A further assumption used in this work concerns the top–bottom symmetry of the double-crossing mode conversion process, i.e., both caustics appear at $k_x=0$ and the wave-coupling strength is assumed to be identical at both single-crossing mode-conversion points. We expect that the modular-eikonal approach would work equally well in the absence of this symmetry, since each single-crossing mode conversion region is solved independently in this approach (see Sec. VI for further comments).

C. Summary of analytical results

We begin by considering the problem of *copropagating* waves. For scenario I ($\epsilon=+1$ and $\kappa=+1$), the \mathbf{S} -matrix relation (23) takes the form

$$\begin{pmatrix} \mathcal{Z}_a^+ \\ \mathcal{Z}_b^+ \end{pmatrix} \equiv \begin{pmatrix} \mathcal{F} & \mathcal{E} \\ -\mathcal{E}^* & \mathcal{F}^* \end{pmatrix} \begin{pmatrix} \mathcal{Z}_a^- \\ \mathcal{Z}_b^- \end{pmatrix} , \quad (25a)$$

where $\mathcal{S}_{aa} \equiv \mathcal{F}$ and $\mathcal{S}_{ab} \equiv \mathcal{E}$, with $|\mathcal{F}|^2 + |\mathcal{E}|^2 = 1$. From (21a) and (21b), with $\kappa\epsilon=+1$, the global transmission and conversion coefficients for scenario I are

$$T_D^I = |\mathcal{F}|^2 \quad \text{and} \quad C_D^I = |\mathcal{E}|^2 . \quad (25b)$$

For scenario III ($\epsilon=-1$ and $\kappa=+1$), on the other hand, the \mathbf{S} -matrix relation (23) becomes

$$\begin{pmatrix} \mathcal{Z}_a^+ \\ \mathcal{Z}_b^+ \end{pmatrix} \equiv \begin{pmatrix} \mathcal{F}' & \mathcal{E}' \\ (\mathcal{E}')^* & (\mathcal{F}')^* \end{pmatrix} \begin{pmatrix} \mathcal{Z}_a^- \\ \mathcal{Z}_b^- \end{pmatrix} , \quad (26a)$$

where $\mathcal{S}_{aa} \equiv \mathcal{F}'$ and $\mathcal{S}_{ab} \equiv \mathcal{E}'$, with $|\mathcal{F}'|^2 - |\mathcal{E}'|^2 = 1$. From (21a) and (21b), with $\kappa\epsilon=-1$, the global transmission and conversion coefficients for scenario III are

$$T_D^{\text{III}} = |\mathcal{F}'|^2 \quad \text{and} \quad C_D^{\text{III}} = -|\mathcal{E}'|^2 . \quad (26b)$$

From the results of the modular-eikonal analysis to be presented in Sec. V, the expressions for $(\mathcal{F}, \mathcal{E})$ and $(\mathcal{F}', \mathcal{E}')$ are

$$\mathcal{F} = T_S + (1 - T_S)e^{2i\Theta_+} , \quad (27a)$$

$$\mathcal{E} = 2ie^{i\theta} \sqrt{T_S(1 - T_S)} \sin \Theta_+ ,$$

and

$$\mathcal{F}' = T_S^{-1} - (T_S^{-1} - 1)e^{2i\Theta_-} , \quad (27b)$$

$$\mathcal{E}' = -2ie^{i\theta} \sqrt{T_S^{-1}(T_S^{-1} - 1)} \sin \Theta_- ,$$

where $T_S \equiv \exp(-2\pi|\nu|^2)$ is the single-crossing (S) transmission coefficient, $\theta \equiv \arg \bar{\eta}$, and

$$\Theta_\epsilon(\Delta X, |\nu|^2) \equiv \frac{2}{3} (\Delta X)^{3/2} + 3\epsilon |\nu|^2 \ln(2\sqrt{\Delta X}) + \epsilon \arg[\Gamma(-i|\nu|^2)] - \frac{\pi}{4}; \quad (27c)$$

here $|\nu|^2 \equiv |\bar{\eta}|^2/2\sqrt{\Delta X}$ and $\arg[\Gamma(-i|\nu|^2)]$ denotes the phase of the gamma function with imaginary argument $-i|\nu|^2$.

Next, we consider double-crossing mode conversion involving two *counterpropagating* waves ($\kappa = -1$). In analyzing scenarios II and IV (with $\epsilon = -1$ and $+1$, respectively), the outgoing amplitudes are now (Z_a^+, Z_b^+) and the incoming amplitudes are (Z_a^-, Z_b^-) . By rearranging the terms in (25a), we obtain the **S**-matrix relation for scenario IV:

$$\begin{pmatrix} Z_a^+ \\ Z_b^- \end{pmatrix} \equiv \begin{pmatrix} 1/\mathcal{S}^* & \mathcal{E}'\mathcal{S}^* \\ \mathcal{E}^*/\mathcal{S}^* & 1/\mathcal{S}^* \end{pmatrix} \begin{pmatrix} Z_a^- \\ Z_b^+ \end{pmatrix}, \quad (28a)$$

where $\mathcal{S}_{aa} = 1/\mathcal{S}^*$ and $\mathcal{S}_{ab} = \mathcal{E}'\mathcal{S}^*$, with $1/|\mathcal{S}|^2 - |\mathcal{E}'|^2/|\mathcal{S}^*|^2 = 1$, which follows from (25b). From (21a) and (21b), with $\kappa\epsilon = -1$, the global transmission and conversion coefficients for scenario IV are

$$T_D^{IV} = 1/|\mathcal{S}|^2 \quad \text{and} \quad C_D^{IV} = -|\mathcal{E}'|^2/|\mathcal{S}^*|^2. \quad (28b)$$

Similarly, by rearranging the terms in (26a), we obtain the following **S**-matrix relation for scenario II:

$$\begin{pmatrix} Z_a^+ \\ Z_b^- \end{pmatrix} \equiv \begin{pmatrix} 1/\mathcal{S}'^* & \mathcal{E}'\mathcal{S}'^* \\ -\mathcal{E}'^*/\mathcal{S}'^* & 1/\mathcal{S}'^* \end{pmatrix} \begin{pmatrix} Z_a^- \\ Z_b^+ \end{pmatrix}, \quad (29a)$$

where $\mathcal{S}_{aa} = 1/\mathcal{S}'^*$ and $\mathcal{S}_{ab} = \mathcal{E}'\mathcal{S}'^*$, with $1/|\mathcal{S}'|^2 + |\mathcal{E}'|^2/|\mathcal{S}'^*|^2 = 1$, which follows from (26b). From (21a) and (21b), with $\kappa\epsilon = +1$, the global transmission and conversion coefficients for scenario II are

$$T_D^{II} = 1/|\mathcal{S}'|^2 \quad \text{and} \quad C_D^{II} = |\mathcal{E}'|^2/|\mathcal{S}'^*|^2. \quad (29b)$$

Using (25b) and (28b), the global transmission coefficients for scenarios I and IV are

$$T_D^I \equiv (T_D^{IV})^{-1} = 1 - 4T_S(1 - T_S)\sin^2 \Theta_+ \leq 1. \quad (30a)$$

Similarly, using (26b) and (29b), the global transmission coefficients for scenarios II and III are

$$T_D^{III} \equiv (T_D^{II})^{-1} = 1 + 4T_S^{-1}(T_S^{-1} - 1)\sin^2 \Theta_- \geq 1. \quad (30b)$$

We note that $T_D^I \equiv (T_D^{IV})^{-1}$ and $T_D^{III} \equiv (T_D^{II})^{-1}$ are exact results that do not depend on the validity of the modular-eikonal approach [from which the right sides of (30a) and (30b) are obtained].

D. Comments concerning scenario IV

Upon further investigation of (30a), we note that, under certain conditions, it is possible to find values of $|\bar{\eta}|^2$ and ΔX for which T_D^I vanishes (and T_D^{IV} becomes infinite). Indeed, when $T_S = 1/2$ and $\sin^2 \Theta_+ = 1$ is substituted in (30a), we find $T_D^I = (T_D^{IV})^{-1} = 0$. From the first condition, we find $|\bar{\eta}|^2/(2\sqrt{\Delta X}) = (\ln 2)/2\pi \equiv |\nu_0|^2$, which can be substituted into the second condition to give $\Theta_+(\Delta X, |\nu_0|^2) = (n + 1/2)\pi$ (for $n \geq 0$). Multiplying this equation by 2, and rearranging some terms, we obtain

$$\begin{aligned} & \frac{4}{3} (\Delta X)^{3/2} + 2 \left(3|\nu_0|^2 \ln(2\sqrt{\Delta X}) + \arg[\Gamma(-i|\nu_0|^2)] - \frac{\pi}{2} \right) \\ & = 2n\pi + \pi/2. \end{aligned} \quad (31)$$

In the limit $|\nu_0|^2 \rightarrow 0$, the left side becomes $(4/3)(\Delta X)^{3/2}$, which is the enclosed area contained between the two crossing uncoupled parabolas [where we used the fact that $\arg[\Gamma(-ia)] \rightarrow \pi/2$ as $a \rightarrow 0$]; we therefore interpret the left side as the enclosed area with finite wave-coupling effects. This equation then states that a precise phase matching at each single-crossing mode conversion must occur as the waves perform one circuit; the term $\pi/2$ on the right side of (31) is the sum of the two (lowest-order) phase shifts at the conversion points.

The possibility of having an infinite transmission coefficient in scenario IV points to the existence of an instability mechanism. In Ref. 5, we studied this instability as an initial value problem based on a modification of (15), where the off-diagonal terms are replaced as follows: $\bar{\eta} \rightarrow \bar{\eta} \exp -\Omega K$, $\bar{\eta}^* \rightarrow \bar{\eta}^* \exp \Omega K$, with the dimensionless growth rate defined as $\Omega \equiv (\Delta\beta)^{-1/3} (|k_x^a|^{-1} + |k_x^b|^{-1})\gamma$. The modified coupled equations are then solved as an eigenvalue problem, where, for a given value of the parameter $|\bar{\eta}|^2$, one solves for the eigenvalue $\Delta X + i\Omega$ by imposing boundary conditions at $K = \pm\infty$. What we then find is that, whenever $\Delta X_{l-1} < \Delta X < \Delta X_l$ (for $l \geq 1$), where ΔX_n are roots of (31), there are l unstable roots, with the ΔX_0 root being the most unstable. We also find that this instability has a threshold $|\bar{\eta}_{\text{th}}|^2 \equiv [(\ln 2)/\pi]\sqrt{\Delta X_0}$. The results of the modular-eikonal approach for this instability agree very well with the numerical study of this instability.⁵

E. Comparison with numerical results

Equation (15) has been solved numerically as a boundary-value problem using the Burlisch–Stoer method:⁸ once incoming boundary conditions are prescribed, the outgoing wave solutions are sought.

Figures 6(a) and 6(b) show a comparison between analytical and numerical results for the transmission coefficients $T_D^I \equiv (T_D^{IV})^{-1}$ and $T_D^{III} \equiv (T_D^{II})^{-1}$, with $|\bar{\eta}|^2 = 0.5$. Solid lines correspond to the numerical solutions of (15) for each scenario, while dotted lines are given by the analytical formulas (30a) and (30b). Excellent agreement between the analytical and numerical results is observed for each scenario whenever $\Delta X > 2$, in agreement with condition (24). Excellent agreement for each scenario was also obtained for other values of $|\bar{\eta}|^2$.

IV. INNER AND OUTER SOLUTIONS

The next two sections present the technical aspects of the derivation of (30a) and (30b) based on the modular-eikonal approach. An important step in this approach involves asymptotic matching between the outer wave solutions (defined in the eikonal regions) and the inner wave solutions (defined in the mode-conversion regions) near each of the two double-crossing mode-conversion points. In the present section, we derive expressions for the outer and inner

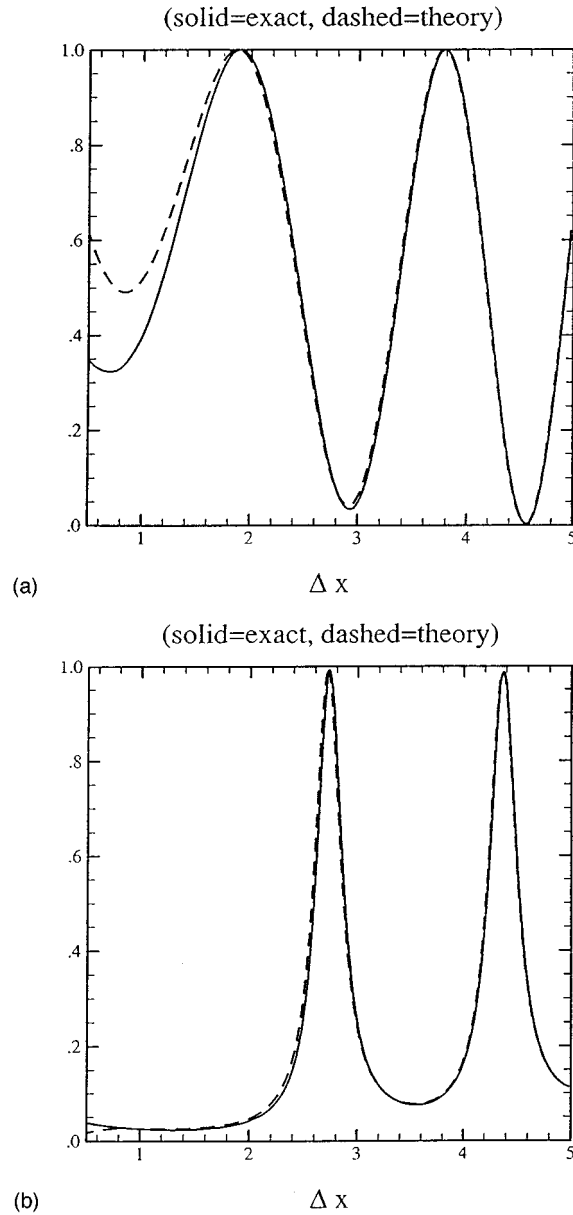


FIG. 6. A comparison of analytical and numerical results for the global transmission coefficient T_D for each scenario as a function of the dimensionless caustic separation ΔX , for dimensionless wave-coupling strength $|\bar{\eta}|^2=0.5$: (a) scenario I; and (b) scenario II. For scenarios III and IV, the global transmission coefficients T_D^{III} and T_D^{IV} satisfy the identities $T_D^{\text{III}} \equiv (T_D^{\text{II}})^{-1}$ and $T_D^{\text{IV}} \equiv (T_D^{\text{I}})^{-1}$.

solutions near these points, while in the next section, we perform the asymptotic matching, leading to (30a) and (30b).

A. Outer solutions

To perform asymptotic matching between the outer and inner solutions near the crossing points, we begin by evaluating $S(K)$ [(17b)] near $(X, K) = (0, \pm\sqrt{\Delta X})$. For this purpose, it is convenient to introduce the local (and rescaled) canonical pair of phase-space coordinates (q, p) , defined by

$$X \equiv (2\sqrt{\Delta X})^{1/2} q, \quad K \equiv \sigma\sqrt{\Delta X} + p/(2\sqrt{\Delta X})^{1/2}, \quad (32)$$

where $\sigma = +1$ represents the top conversion while $\sigma = -1$ represents the bottom conversion (the rescaling of p and q is

introduced to simplify the algebra). Using these coordinates, in the limit where $|p|^2 \ll (\Delta X)^{3/2}$ and $|\nu|^2 \ll (\Delta X)^{3/2}$, the expression for $S(K)$ near the conversion points is $S(K) \equiv -\sigma[S_\epsilon(p) - \varphi_\epsilon] + \mathcal{O}[(\Delta X)^{-3/4}]$, where

$$S_\epsilon(p) \equiv \frac{p^2}{4} + \epsilon|\nu|^2 \ln|p| \quad \text{and} \\ \varphi_\epsilon \equiv \frac{(\Delta X)^{3/2}}{3} + \frac{3\epsilon|\nu|^2}{2} \ln 2\sqrt{\Delta X}. \quad (33)$$

Hence, near the conversion points, the eikonal solutions (17a) become the *outer* solutions:

$$\psi_j^{\text{outer}}(p) = (Z_j^\alpha e^{\mp i\sigma\varphi_\epsilon}) e^{\pm i\sigma S_\epsilon(p)}, \quad (34)$$

where the eikonal-region label α is either $-$, 0 , or $+$, and the upper (lower) sign refers to wave a (wave b). Now that the outer solutions (in the eikonal regions) are known, we turn our attention to the solutions of the coupled-wave equations in the mode-conversion regions (the *inner* solutions).

B. Inner solutions

The study of the inner solutions is based on the solutions of the single-crossing mode-conversion problem. The \mathbf{S} matrix for a general single-crossing mode conversion was first obtained by Tracy and Kaufman⁹ by using metaplectic-transform techniques.

We begin by linearizing the dispersion matrix in (15) about the crossing points at $(X=0, K=\pm\sqrt{\Delta X})$. For this purpose, we use the canonical coordinates (32). When these coordinates are substituted into (15), we obtain, after linearizing in p ,

$$\begin{pmatrix} \epsilon_a(\hat{q} + \sigma p/2) & \nu \\ \nu^* & \epsilon_b(\hat{q} - \sigma p/2) \end{pmatrix} \begin{pmatrix} \psi_a(p) \\ \psi_b(p) \end{pmatrix} = 0, \quad (35)$$

where $\hat{q} = id/dp$. In the neighborhood of both single crossings, the *uncoupled* parabolic rays are thus approximated as straight lines: $p(q) = \pm 2q$.

Locally, one can choose (following Tracy and Kaufman) new canonically conjugate coordinates $Q \equiv Q(q, p)$ and $P \equiv P(q, p)$, such that $\{Q, P\} = +1$ and Q or P vanishes when $p(q) = +2q$ or $p(q) = -2q$. For scenarios I and IV (where $\epsilon_a = +1 = \epsilon_b$), we choose

$$Q \equiv (q + p/2), \quad P \equiv -(q - p/2), \quad (36)$$

for both single crossings. For scenarios II and III (where $\epsilon_a = +1 = -\epsilon_b$), on the other hand, we choose

$$Q \equiv -\sigma(q - p/2), \quad P \equiv -\sigma(q + p/2). \quad (37)$$

The local (Q, P) frames, given by (36) and (37), are shown in Figs. 7(a) and 7(b) superposed onto the dispersion curves.

After substituting the new canonical coordinates (Q, P) into (35), two distinct formulations of single-crossing mode conversion are obtained. The first formulation, labeled a Q_a type, describes the situation where wave a asymptotically lives on the Q axis (while wave b asymptotically lives on the P axis). The single-crossing mode-conversion equations are [from (35)]

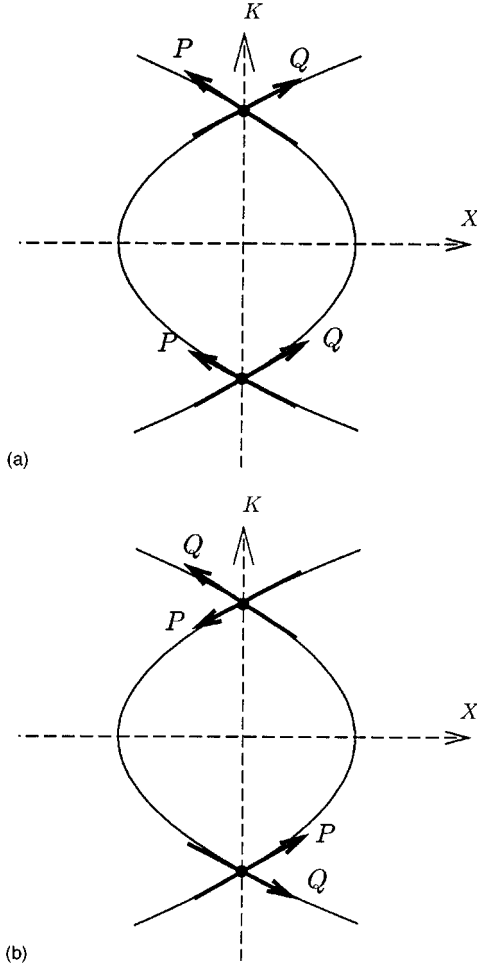


FIG. 7. (Q, P) -frames for (a) scenarios I and IV, and (b) scenarios II and III. Note that a wave crossing a mode-conversion point on the Q axis crosses the other mode conversion point on the P axis (or vice versa).

$$\begin{pmatrix} -\hat{P} & \nu \\ \nu^* & Q \end{pmatrix} \begin{pmatrix} \bar{\psi}_a(Q) \\ \bar{\psi}_b(Q) \end{pmatrix} = 0, \quad (38)$$

where $\hat{P} \equiv -id/dQ$. The Q_a -type conversion is found in the bottom conversion of scenarios I and IV, and the top conversion of scenarios II and III. The second formulation, labeled a Q_b type, describes the situation where wave b lives on the Q axis (while wave a lives on the P axis). The single-crossing mode-conversion equations are [from (35)]

$$\begin{pmatrix} Q & \nu \\ \nu^* & -\hat{P} \end{pmatrix} \begin{pmatrix} \bar{\psi}_a(Q) \\ \bar{\psi}_b(Q) \end{pmatrix} = 0. \quad (39)$$

The Q_b -type conversion is found in the top conversion of scenarios I and IV, and the bottom conversion of scenarios II and III. (Note that each double-crossing mode conversion diagram is described in terms of single-crossing mode conversions of each of these two types.¹⁰)

The solutions of the single-crossing mode conversion problems of both types are presented in Appendix C and only results are summarized here. The solutions for the Q_a type are $\bar{\psi}_a(Q)$ and $\bar{\psi}_b(P)$, while the solutions for the Q_b type are $\bar{\psi}_a(P)$ and $\bar{\psi}_b(Q)$, where

$$\bar{\psi}_j(Q) = \begin{cases} z_j^{\text{out}} Q^{-i|\nu|^2}, & Q > 0, \\ z_j^{\text{in}} |Q|^{-i|\nu|^2}, & Q < 0, \end{cases} \quad (40)$$

for $Q \neq 0$, and

$$\bar{\psi}_j(P) \equiv \begin{cases} z_j^{\text{out}} P^{i|\nu|^2}, & P > 0, \\ z_j^{\text{in}} |P|^{i|\nu|^2}, & P < 0, \end{cases} \quad (41)$$

for $P \neq 0$ (note that mode conversion occurs at $Q=0=P$); in (40)–(41), the amplitudes ($z_j^{\text{out}}, z_j^{\text{in}}$) are either $(a_{\text{out}}, a_{\text{in}})$ or $(b_{\text{out}}, b_{\text{in}})$. The \mathbf{S} -matrix relation between the incoming amplitudes $(a_{\text{in}}, b_{\text{in}})$ and the outgoing amplitudes $(a_{\text{out}}, b_{\text{out}})$ is

$$\begin{pmatrix} a_{\text{out}} \\ b_{\text{out}} \end{pmatrix} \equiv \begin{pmatrix} \sqrt{T_S} & -\sqrt{1-T_S} e^{i(\phi \pm \theta)} \\ \sqrt{1-T_S} e^{-i(\phi \pm \theta)} & \sqrt{T_S} \end{pmatrix} \begin{pmatrix} a_{\text{in}} \\ b_{\text{in}} \end{pmatrix}, \quad (42)$$

where the upper and lower signs refer to waves a and b , respectively, the single-crossing transmission coefficient T_S is defined above and $\phi \equiv \pi/4 - \arg \Gamma(-i|\nu|^2)$.

C. Metaplectic transforms

Our next step involves transforming the mode-conversion solutions (40)–(41) into functions of p . To perform this transformation, we use the metaplectic transforms^{11,12}

$$\begin{aligned} \psi_j^{\text{inner}}(p) &\equiv \int_{-\infty}^{+\infty} dQ \left(\frac{-1}{2\pi i} \frac{\partial^2 F_3(p, Q)}{\partial p \partial Q} \right)^{1/2} \\ &\times e^{iF_3(p, Q)} \bar{\psi}_j(Q), \end{aligned} \quad (43)$$

and

$$\begin{aligned} \psi_j^{\text{inner}}(p) &\equiv \int_{-\infty}^{+\infty} dP \left(\frac{-1}{2\pi i} \frac{\partial^2 F_4(p, P)}{\partial p \partial P} \right)^{1/2} \\ &\times e^{iF_4(p, P)} \bar{\psi}_j(P), \end{aligned} \quad (44)$$

where $F_3(p, Q)$ and $F_4(p, P)$ are generating functions for a canonical transformation from the ‘‘old’’ coordinates (q, p) to the ‘‘new’’ coordinates (Q, P) ; see Ref. 13 for further details on generating functions. The metaplectic transforms (43)–(44) are performed explicitly in Appendix D; only the results are shown here. For the case $\epsilon = +1$, we obtain

$$\psi_j^{\text{inner}}(p) = e^{\mp iS_+(p)} \begin{cases} z_j^{\text{out}}, & p > 0, \\ z_j^{\text{in}}, & p < 0, \end{cases} \quad (45)$$

where the upper and lower signs refer to (43) and (44), respectively. For $\epsilon = -1$, we obtain

$$\psi_j^{\text{inner}}(p) = \sqrt{\pm \sigma} e^{\pm iS_-(p)} \begin{cases} z_j^{\text{out}}, & \sigma p > 0, \\ z_j^{\text{in}}, & \sigma p < 0. \end{cases} \quad (46)$$

We are now ready to perform the asymptotic matching between the outer solutions (34) and the inner solutions (45) or (46). This task is performed in the next section.

V. MODULAR-EIKONAL ANALYSIS OF THE FOUR SCENARIOS

In this section, the modular-eikonal analysis of each of the four scenarios is performed by asymptotic matching of the outer and inner solutions at both double-crossing mode-

conversion points. This matching procedure yields the single-crossing top and bottom \mathbf{S} matrices, which are then used to obtain the global \mathbf{S} matrix from (23). For the sake of brevity, we present the case of scenario I in detail while the other scenarios are summarized.

A. Top conversion of scenario I

The top conversion of scenario I is a Q_b -type conversion. The outer solutions are [from (34) with $\sigma = +1$ and $\epsilon = +1$]

$$\psi_j^{\text{outer}}(p) = e^{\pm i[S_+(p) - \varphi_+]} \begin{cases} Z_j^+, & p > 0, \\ Z_j^0, & p < 0, \end{cases} \quad (47)$$

where $S_+(p)$ and φ_+ are defined in (33), and the upper (lower) sign [here and in (48)] refers to wave a (wave b). The inner solutions are

$$\psi_j^{\text{inner}}(p) = e^{\pm iS_+(p)} \begin{cases} z_j^+, & p > 0, \\ z_j^0, & p < 0. \end{cases} \quad (48)$$

The \mathbf{S} -matrix relation between the incoming asymptotic amplitudes (b_0, a_0) and the outgoing asymptotic amplitudes (b_+, a_+) is [from (42) with a lower sign]

$$\begin{pmatrix} b_+ \\ a_+ \end{pmatrix} = \begin{pmatrix} \sqrt{T_S} & -\sqrt{1-T_S}e^{i(\phi-\theta)} \\ \sqrt{1-T_S}e^{-i(\phi-\theta)} & \sqrt{T_S} \end{pmatrix} \begin{pmatrix} b_0 \\ a_0 \end{pmatrix}. \quad (49)$$

By matching (47) with (48), we find the following relations between the inner and outer solutions for waves a and b : $(a_0, a_+) \equiv (Z_a^0, Z_a^+)e^{-i\varphi_+}$ and $(b_0, b_+) \equiv (Z_b^0, Z_b^+)e^{i\varphi_+}$. By substituting these relations into (49), we obtain (after some straightforward manipulations) the \mathbf{S} matrix \mathbf{S}_{top} involved in the relation between the incoming asymptotic state (Z_a^0, Z_b^0) and the outgoing asymptotic state (Z_a^+, Z_b^+) for the top crossing of scenario I:

$$\mathbf{S}_{\text{top}} \equiv \begin{pmatrix} \sqrt{T_S} & \sqrt{1-T_S}e^{i(\Theta_+ + \theta)} \\ -\sqrt{1-T_S}e^{-i(\Theta_+ + \theta)} & \sqrt{T_S} \end{pmatrix}, \quad (50)$$

$$\mathbf{S}_{\text{global}} \equiv \begin{pmatrix} T_S + (1-T_S)e^{2i\Theta_+} & 2ie^{i\theta}\sqrt{T_S(1-T_S)} \sin \Theta_+ \\ 2ie^{-i\theta}\sqrt{T_S(1-T_S)} \sin \Theta_+ & T_S + (1-T_S)e^{-2i\Theta_+} \end{pmatrix}. \quad (51)$$

A comparison with (25a) yields the global transmission and conversion amplitudes (27a) for scenario I. These expressions are then used to obtain the global transmission coefficients for scenarios I and IV, as shown in (30a).

Following a similar procedure, the global \mathbf{S} matrix for scenario III is

$$\mathbf{S}_{\text{global}} \equiv \begin{pmatrix} T_S^{-1} - (T_S^{-1} - 1)e^{2i\Theta_-} & -2ie^{i\theta}\sqrt{T_S^{-1}(T_S^{-1} - 1)} \sin \Theta_- \\ 2ie^{-i\theta}\sqrt{T_S^{-1}(T_S^{-1} - 1)} \sin \Theta_- & T_S^{-1} - (T_S^{-1} - 1)e^{-2i\Theta_-} \end{pmatrix}, \quad (56)$$

where $\Theta_- \equiv 2\varphi_- + \phi$ [see (27c)]. Comparison with (26a) yields the global transmission and conversion amplitudes (27b) for scenario III. These expressions are then used to obtain the global transmission coefficients for scenarios II and III, as shown in (30b).

where $\Theta_+ \equiv 2\varphi_+ - \phi$ [see (27c)].

B. Bottom conversion of scenario I

The bottom conversion of scenario I is a Q_a -type conversion. The outer solutions are [from (34) with $\sigma = -1$ and $\epsilon = +1$]

$$\psi_j^{\text{outer}}(p) = e^{\mp i[S_+(p) - \varphi_+]} \begin{cases} Z_j^0, & p > 0, \\ Z_j^-, & p < 0, \end{cases} \quad (51)$$

while the inner solutions are

$$\psi_j^{\text{inner}}(p) = e^{\mp iS_+(p)} \begin{cases} z_j^0, & p > 0, \\ z_j^-, & p < 0, \end{cases} \quad (52)$$

where the upper and lower signs in (51)–(52) refer to wave a and wave b , respectively. The \mathbf{S} -matrix relation between the incoming asymptotic amplitudes (a_-, b_-) and the outgoing asymptotic amplitudes (a_0, b_0) is [from (42) with an upper sign]

$$\begin{pmatrix} a_0 \\ b_0 \end{pmatrix} = \begin{pmatrix} \sqrt{T_S} & -\sqrt{1-T_S}e^{i(\phi+\theta)} \\ \sqrt{1-T_S}e^{-i(\phi+\theta)} & \sqrt{T_S} \end{pmatrix} \begin{pmatrix} a_- \\ b_- \end{pmatrix}. \quad (53)$$

By matching (51)–(52), we find $(a_0, a_-) \equiv (Z_a^0, Z_a^-)e^{i\varphi_+}$ and $(b_0, b_-) \equiv (Z_b^0, Z_b^-)e^{-i\varphi_+}$. By substituting these relations into (53), we obtain, after some straightforward manipulations, the \mathbf{S} matrix for the bottom conversion of scenario I:

$$\mathbf{S}_{\text{bottom}} \equiv \begin{pmatrix} \sqrt{T_S} & -\sqrt{1-T_S}e^{i(\Theta_+ - \theta)} \\ \sqrt{1-T_S}e^{i(\Theta_+ - \theta)} & \sqrt{T_S} \end{pmatrix}. \quad (54)$$

C. Global double-crossing mode conversion

We now combine, following (23), the top and bottom \mathbf{S} matrices, (50) and (54), to obtain the *global* \mathbf{S} matrix for scenario I:

VI. DISCUSSION

We conclude our work by reviewing our results and by discussing the assumptions used in the modular-eikonal approach and its extensions.

Our purpose was to study the effects of ray curvature on mode conversion. This led us to consider double-crossing mode conversion in the neighborhood of two caustics. As demonstrated by our analytical results (based on the modular-eikonal approach), ray curvature introduces destructive and constructive interference effects in wave transmission through a double-crossing mode-conversion region. By comparing these results with numerical solutions of the coupled-wave equations, we have confirmed these effects and established the validity of the modular-eikonal approach. Our theory shows that interference effects depend on only two dimensionless parameters: the dimensionless caustic separation ΔX and the dimensionless wave-coupling strength $\bar{\eta}$. Four scenarios were identified: each scenario was distinguished on the basis of whether the two coupled waves had the same or opposite energy signs, and whether they were copropagating or counterpropagating in k_x . One of the scenarios (counterpropagating waves with opposite energy signs) also led to the discovery of a new instability mechanism.

For a given double-crossing scenario, the wave equations are parametrized by $(\eta, \Delta x, \Delta \beta)$, where η is the wave-coupling strength (evaluated at the crossing points), Δx is the separation between the two caustics, and $\Delta \beta$ is the ray curvature between the two waves. We observed (in Appendix A) that, for the modular-eikonal approach to be valid, the caustic separation Δx and the wave-coupling strength η had to satisfy

$$\Delta x \gg |\eta| |(\partial_x D_a)_0 (\partial_x D_b)_0|^{-1/2}, \quad (57)$$

which is (24) in dimensional form. This condition was necessary for both waves to enter their eikonal regimes before reaching $k_x = 0$, the midpoint between the two crossing points $k_x = \pm (\Delta x / \Delta \beta)^{1/2}$.

The even parity of both dispersion functions in k_x (assumed in this work) leads to the top–bottom symmetry of the double-crossing mode-conversion picture. What this means is that the (dimensionless) parameter list $(\Delta X, \bar{\eta})$ is the same at both single-crossing (top and bottom) mode-conversion points. Top–bottom symmetry is broken, for example, when the two uncoupled rays have the form $x_a(k_x) = x_{a0} + \beta_a k_x^2$ and $x_b(k_x) = x_{b0} + \alpha_b k_x$, where wave b has negligible curvature compared to the linear term $\alpha_b k_x$. This situation means that the two rays cross at $(x^{\text{bottom}}, k_x^{\text{bottom}})$ and $(x^{\text{top}}, k_x^{\text{top}})$, where

$$k_x^{\text{top, bottom}} = \frac{\alpha_b}{2\beta_a} \left(\pm \sqrt{1 + \frac{4\beta_a \Delta x}{\alpha_b^2}} - 1 \right), \quad (58)$$

where $\Delta x \equiv x_{a0} - x_{b0}$, and $x^{\text{top}} \equiv x_j(k_x^{\text{top}})$, $x^{\text{bottom}} \equiv x_j(k_x^{\text{bottom}})$, where j is either a or b . Since the crossings occur at different k_x values, the wave-coupling strength is expected to be different at both crossings, i.e., $\eta_{\text{top}} \neq \eta_{\text{bottom}}$. Since the modular-eikonal approach considers the two single-crossing mode conversions independently of each other, the different parametrizations at these crossings does not jeopardize its applicability; the new intermediate eikonal region is now centered at the midpoint between k_x^{bottom} and k_x^{top} , i.e., $k_x = -\alpha_b / (2\beta_a)$. Hence we expect that, even in

the absence of top–bottom symmetry, the modular-eikonal approach can be used to study more general double-crossing mode-conversion problems.

ACKNOWLEDGMENT

This work was supported by U.S. Department of Energy Contract No. DE-AC03-76SFO0098.

APPENDIX A: EIKONAL SOLUTIONS OF THE COUPLED-WAVE EQUATIONS (15)

The purpose of this appendix is to present a complete derivation of (17a) and (17b) by asymptotic analysis of the solutions of the coupled wave equations (15):

$$i \frac{d\psi_a}{dK}(K) - \Phi'(K) \psi_a(K) = -\epsilon_a \bar{\eta} \psi_b(K), \quad (A1)$$

$$i \frac{d\psi_b}{dK}(K) + \Phi'(K) \psi_b(K) = -\epsilon_b \bar{\eta}^* \psi_a(K), \quad (A2)$$

where

$$\Phi(K) \equiv \frac{1}{2} K \Delta X - \frac{1}{6} K^3. \quad (A3)$$

In the absence of wave coupling ($\bar{\eta} = 0$), the solutions of (A1)–(A2) are $\psi_j(K) \equiv Z_j e^{\mp i\Phi(K)}$, where Z_j ($j = a, b$) are (global) constants and $\Phi(K)$ is the (exact) eikonal phase. For the sake of brevity, upper and lower signs (i.e., \pm or \mp) always refer to wave a and wave b , respectively. When wave-coupling effects are considered, the solutions of (A1)–(A2) are written in the form $\psi_j(K) \equiv \tilde{\psi}_j(K) e^{\mp i\Phi(K)}$, where $\tilde{\psi}_j(K)$ satisfies the second-order equation:

$$\frac{d}{dK} \left(e^{\mp 2i\Phi(K)} \frac{d\tilde{\psi}_j}{dK}(K) \right) = -\epsilon |\bar{\eta}|^2 e^{\mp 2i\Phi(K)} \tilde{\psi}_j(K), \quad (A4)$$

where $\epsilon \equiv \epsilon_a \epsilon_b$.

We now wish to solve (A4) in three *asymptotic* regions represented by the limits $K \rightarrow \pm \infty$ and $K \rightarrow 0$, corresponding to the upper asymptotic region (labeled $\alpha = +$), the lower asymptotic region (labeled $\alpha = -$), and the intermediate asymptotic region (labeled $\alpha = 0$), respectively. In each asymptotic region α (for fixed $|\bar{\eta}|^2$), we look for solutions of the form

$$\tilde{\psi}_j^\alpha(K) \equiv Z_j^\alpha e^{\mp i\phi_j^\alpha(K)}, \quad (A5)$$

where Z_j^α ($j = a, b$) are constant within the asymptotic region α , and $\phi_j^\alpha(K)$ are complex-valued phase *perturbations*, which satisfy the boundary conditions

$$\begin{aligned} \phi_j^+(K \rightarrow +\infty) &= 0, & \phi_j^0(K = 0) &= 0, & \text{and} \\ \phi_j^-(K \rightarrow -\infty) &= 0. \end{aligned} \quad (A6)$$

Substitution of (A5) into (A4) yields

$$\pm i \frac{d^2 \phi_j^\alpha}{dK^2} + \left(\Delta X - K^2 + \frac{d\phi_j^\alpha}{dK} \right) \frac{d\phi_j^\alpha}{dK} = \epsilon |\bar{\eta}|^2. \quad (A7)$$

We now proceed with the solutions of (A7) in each of the three asymptotic regions.

As the waves enter the asymptotic region α , we expect the phase perturbations ϕ_j^α to become slowly varying functions of K and asymptotically approach zero to satisfy (A6). Consequently, in each asymptotic region, we use the orderings

$$|d\phi_j^\alpha/dK| \ll |\Delta X - K^2| \quad \text{and} \quad |d^2\phi_j^\alpha/dK^2| \ll |(\Delta X - K^2)d\phi_j^\alpha/dK|. \quad (\text{A8})$$

Based on these orderings, we expand $\phi_j^\alpha(K)$: $\phi_j^\alpha(K) = \phi_{j0}^\alpha(K) + \phi_{j1}^\alpha(K) + \dots$, where $|d\phi_{j1}^\alpha/dK| \ll |d\phi_{j0}^\alpha/dK|$. To lowest order in the orderings, (A7) yields

$$\frac{d\phi_{j0}^\alpha}{dK}(K) = \frac{\epsilon|\bar{\eta}|^2}{\Delta X - K^2}. \quad (\text{A9})$$

In all three asymptotic regions, the solutions of (A9) [subject to (A6)] are

$$\phi_{j0}^\alpha(K) \equiv \frac{\epsilon|\bar{\eta}|^2}{2\sqrt{\Delta X}} \ln\left(\frac{|K + \sqrt{\Delta X}|}{|K - \sqrt{\Delta X}|}\right). \quad (\text{A10})$$

(Note that the lowest-order phase perturbations are independent of the asymptotic-region label α and the wave-type label j .) Using (A10), the ordering $|d\phi_{j0}^\alpha/dK| \ll |\Delta X - K^2|$ becomes $|\Delta X - K^2| \gg |\bar{\eta}|$, which is easily satisfied in the upper and lower asymptotic regions (where $K \rightarrow \pm\infty$). In the intermediate asymptotic region (where $K \rightarrow 0$), we obtain instead

$$|\Delta X| \gg |\bar{\eta}|, \quad (\text{A11})$$

i.e., the caustic separation must be large enough (for given coupling) to allow the waves to enter the eikonal regime.

At the next order, we find from (A7),

$$\frac{d\phi_{j1}^\alpha}{dK}(K) = \frac{-1}{(\Delta X - K^2)^3} (|\bar{\eta}|^4 \pm 2i\epsilon|\bar{\eta}|^2 K). \quad (\text{A12})$$

We now solve (A12) in each of the three asymptotic regions. Note that, in contrast to the lowest-order phase perturbations (A10), the next-order perturbations are complex valued, which means that the asymptotic amplitudes are perturbed as well at this order.

1. Upper and lower asymptotic regions $K \rightarrow \pm\infty$

The solutions of (A12) for $|K| \rightarrow \infty$ ($\alpha = +$ or $-$) are

$$\phi_{j1}^\alpha(K) = \pm \frac{i\epsilon|\bar{\eta}|^2}{2K^4} \left(1 + \frac{2\Delta X}{K^2} + \dots\right) - \frac{|\bar{\eta}|^4}{K^5} \left(\frac{1}{5} + \frac{3\Delta X}{7K^2} + \dots\right). \quad (\text{A13})$$

Hence, the solutions of (A1)–(A2) in the upper and lower asymptotic regions are

$$\psi_j^\alpha(K) \equiv Z_j^\alpha \left(1 = \frac{\epsilon|\bar{\eta}|^2}{2K^4} \pm i \frac{|\bar{\eta}|^4}{5K^5} + \dots\right) e^{\mp iS(K)}, \quad (\text{A14})$$

where, combining (A3) and (A10), the generalized eikonal phase is

$$S(K) \equiv \frac{1}{2} K \Delta X - \frac{1}{6} K^3 + \frac{\epsilon|\bar{\eta}|^2}{2\sqrt{\Delta X}} \ln\left(\frac{|K + \sqrt{\Delta X}|}{|K - \sqrt{\Delta X}|}\right). \quad (\text{A15})$$

Note that the eikonal phase is independent of the asymptotic-region label α .

2. Intermediate asymptotic region $K \rightarrow 0$

In the intermediate asymptotic region, for $|K| \rightarrow 0$ and $\Delta X \gg |\bar{\eta}|$, the solutions of (A12) are

$$\phi_{j1}^0(K) = \frac{-1}{(\Delta X)^3} (\pm i\epsilon|\bar{\eta}|^2 K^2 + |\bar{\eta}|^4 K + \dots). \quad (\text{A16})$$

In the intermediate asymptotic region, the solutions of (A1)–(A2) are

$$\psi_j^0(K) = Z_j^0 \left[1 - \frac{1}{(\Delta X)^3} (\epsilon|\bar{\eta}|^2 K^2 \mp i|\bar{\eta}|^4 K + \dots)\right] e^{\mp iS(K)}. \quad (\text{A17})$$

3. Global asymptotic analysis

In conclusion, we find, from (A14) and (A17), that the lowest-order asymptotic form for the wave fields $\psi_j(K)$ in each of the three asymptotic regions are

$$\psi_j^\alpha(K) \rightarrow e^{\mp iS(K)} \begin{cases} Z_j^+, & \text{for } K \rightarrow +\infty, \\ Z_j^0, & \text{for } K \rightarrow 0, \\ Z_j^-, & \text{for } K \rightarrow -\infty, \end{cases} \quad (\text{A18})$$

where the upper sign in the eikonal phase corresponds to wave a while the lower sign corresponds to wave b . This expression appears in (17a) and (17b) and is used in the wave-action conservation law (18).

APPENDIX B: DERIVATION OF GENERIC S MATRIX

The \mathbf{S} matrix appearing in (20a) has the general form

$$\mathbf{S}_\kappa \equiv \begin{pmatrix} \mathcal{S}_{aa} & \mathcal{S}_{ab} \\ \mathcal{S}_{ba} & \mathcal{S}_{bb} \end{pmatrix}. \quad (\text{B1})$$

For the norm defined in (19a) and (19b), we introduce the metric

$$\mathbf{g} \equiv \begin{pmatrix} 1 & 0 \\ 0 & \kappa\epsilon \end{pmatrix}, \quad (\text{B2})$$

so that

$$\|\mathbf{Z}\|_\kappa^2 \equiv \mathbf{Z}^\dagger \cdot \mathbf{g} \cdot \mathbf{Z}, \quad (\text{B3})$$

where \mathbf{Z}^\dagger denotes the adjoint of \mathbf{Z} . From the conservation law $\|\mathbf{Z}^{\text{out}}\|_\kappa^2 = \|\mathbf{Z}^{\text{in}}\|_\kappa^2$, we find that the \mathbf{S} matrix must satisfy $\mathbf{S}_\kappa^\dagger \cdot \mathbf{g} \cdot \mathbf{S}_\kappa \equiv \mathbf{g}$, and thus the determinant of \mathbf{S}_κ must be

$$\mathcal{S}_{aa}\mathcal{S}_{bb} - \mathcal{S}_{ab}\mathcal{S}_{ba} = \pm 1. \quad (\text{B4})$$

Since the results of the present analysis are independent of the sign of the determinant of \mathbf{S}_κ , we arbitrarily choose the determinant to be $+1$.

Substituting (B1) into (19a) and (19b), we find for $\|\mathbf{Z}^{\text{out}}\|_\kappa^2$,

$$\begin{aligned} \|\mathbf{Z}^{\text{out}}\|_{\kappa}^2 &= (|\mathcal{S}_{aa}|^2 + \kappa\epsilon|\mathcal{S}_{ba}|^2)|Z_a^{\text{in}}|^2 \\ &+ (|\mathcal{S}_{ab}|^2 + \kappa\epsilon|\mathcal{S}_{bb}|^2)|Z_b^{\text{in}}|^2 \\ &+ \text{Re}[(\mathcal{S}_{aa}\mathcal{S}_{ab}^* + \kappa\epsilon\mathcal{S}_{ba}\mathcal{S}_{bb}^*)Z_a^{\text{in}}(Z_b^{\text{in}})^*], \end{aligned} \quad (\text{B5})$$

so that (19a) and (19b) hold only if $|\mathcal{S}_{aa}|^2 + \kappa\epsilon|\mathcal{S}_{ba}|^2 = 1$, $|\mathcal{S}_{bb}|^2 + \kappa\epsilon|\mathcal{S}_{ab}|^2 = 1$, and $\mathcal{S}_{aa}\mathcal{S}_{ab}^* + \kappa\epsilon\mathcal{S}_{ba}\mathcal{S}_{bb}^* = 0$. These three relations, with (B4), yield

$$\mathcal{S}_{bb} = \mathcal{S}_{aa}^* \quad \text{and} \quad \mathcal{S}_{ba} = -\kappa\epsilon\mathcal{S}_{ab}^*, \quad (\text{B6})$$

and (B1) becomes

$$\mathbf{S}_{\kappa} \equiv \begin{pmatrix} \mathcal{S}_{aa} & \mathcal{S}_{ab} \\ -\kappa\epsilon\mathcal{S}_{ab}^* & \mathcal{S}_{aa}^* \end{pmatrix}, \quad (\text{B7})$$

where \mathcal{S}_{aa} and \mathcal{S}_{ab} satisfy

$$|\mathcal{S}_{aa}|^2 + \kappa\epsilon|\mathcal{S}_{ab}|^2 = 1. \quad (\text{B8})$$

We note that, for $\kappa\epsilon = +1$ (i.e., waves with equal energy signs) in (B2), the relation (B3) implies that \mathbf{S}_{κ} is unitary, since $\mathbf{g} \equiv \mathbf{I}$ (the unit matrix) and (B3) becomes $\mathbf{S}_{\kappa}^{\dagger} \cdot \mathbf{S}_{\kappa} = \mathbf{I}$. On the other hand, for $\kappa\epsilon = -1$ (i.e., waves with opposite energy signs) in (B2), (B3) implies that \mathbf{S}_{κ} is no longer unitary in the standard sense, but instead it satisfies $\mathbf{S}_{\kappa}^{\dagger} \cdot \boldsymbol{\sigma} \cdot \mathbf{S}_{\kappa} = \boldsymbol{\sigma}$, where $\boldsymbol{\sigma}$ is defined by (B2) with $\kappa\epsilon = -1$. This *pseudounitariness* condition for waves of opposite energy signs has been observed previously in a different context.⁷

APPENDIX C: SINGLE-CROSSING MODE CONVERSION

The analysis presented in this appendix follows the work of Tracy and Kaufman.⁹

1. Q_a -type single-crossing mode conversion

We begin with the single-crossing conversion in which wave a lives on the Q axis (the Q_a type), represented by the coupled equations (38):

$$\begin{aligned} i d\bar{\psi}_a(Q)/dQ &= -\nu\bar{\psi}_b(Q) \quad \text{and} \\ \nu^*\bar{\psi}_a(Q) &= -Q\bar{\psi}_b(Q). \end{aligned} \quad (\text{C1})$$

After substituting the solution of the second equation of (C1) into the first one, one obtains an ordinary differential equation for $\bar{\psi}_a(Q)$:

$$\frac{d\bar{\psi}_a(Q)}{dQ} = \frac{-i|\nu|^2}{Q} \bar{\psi}_a(Q), \quad (\text{C2})$$

whose solution (for $Q \neq 0$) is expressed as⁹

$$\bar{\psi}_a(Q) = \begin{cases} a_{\text{out}}Q^{-i|\nu|^2}, & Q > 0, \\ a_{\text{in}}|Q|^{-i|\nu|^2}, & Q < 0. \end{cases} \quad (\text{C3})$$

The solution for mode b is obtained from the second equation in (C1). Since wave b asymptotically lives on the P axis, however, we must use the Fourier transform $\bar{\psi}_b(Q) \rightarrow \bar{\psi}_b(P)$, defined as follows:

$$\begin{aligned} \bar{\psi}_b(P) &\equiv \frac{1}{(2\pi i)^{1/2}} \int_{-\infty}^{+\infty} dQ e^{-iPQ} \bar{\psi}_b(Q) \\ &= \frac{-\nu^*}{(2\pi i)^{1/2}} \int_{-\infty}^{+\infty} \frac{dQ}{Q} \bar{\psi}_a(Q) e^{-iPQ} \\ &= \frac{-\nu^*}{(2\pi i)^{1/2}} \int_0^{+\infty} dQ Q^{-i|\nu|^2-1} (e^{-iPQ} a_{\text{out}} \\ &\quad - e^{iPQ} a_{\text{in}}), \end{aligned} \quad (\text{C4})$$

where the unconventional phase factor $i^{-1/2}$ appearing on the right side is included for consistency with the metaplectic transforms.¹¹ The integration in (C4) can be done explicitly in terms of the Gamma function, and we find⁹

$$\bar{\psi}_b(P) = \frac{-\nu^*\Gamma(-i|\nu|^2)}{(2\pi i)^{1/2}} [a_{\text{out}}(iP)^{i|\nu|^2} - a_{\text{in}}(-iP)^{i|\nu|^2}].$$

Expressing the solution for wave b on the P axis (for $P \neq 0$) as

$$\bar{\psi}_b(P) \equiv \begin{cases} b_{\text{out}}P^{i|\nu|^2}, & P > 0, \\ b_{\text{in}}|P|^{i|\nu|^2}, & P < 0, \end{cases} \quad (\text{C5})$$

we find, defining $\tau \equiv e^{-\pi|\nu|^2}$, with $(\pm i)^{i|\nu|^2} \equiv \tau^{\mp 1/2}$, and $\rho \equiv (2\pi i\tau)^{1/2}/[\nu^*\Gamma(-i|\nu|^2)]$ (with $|\rho|^2 = 1 - \tau^2$): $b_{\text{out}} = (a_{\text{in}} - \tau a_{\text{out}})/\rho$ and $b_{\text{in}} = (\tau a_{\text{in}} - a_{\text{out}})/\rho$. From these equations, one obtains the \mathbf{S} -matrix relation between the incoming amplitudes ($a_{\text{in}}, b_{\text{in}}$) and the outgoing amplitudes ($a_{\text{out}}, b_{\text{out}}$):

$$\begin{pmatrix} a_{\text{out}} \\ b_{\text{out}} \end{pmatrix} \equiv \begin{pmatrix} \tau & -\rho \\ \rho^* & \tau \end{pmatrix} \begin{pmatrix} a_{\text{in}} \\ b_{\text{in}} \end{pmatrix}. \quad (\text{C6})$$

2. Q_b -type single-crossing mode conversion

In the case where wave b lives on the Q axis (the Q_b type), the coupled equations (39) are

$$\begin{pmatrix} id/dQ & \nu^* \\ \nu & Q \end{pmatrix} \begin{pmatrix} \bar{\psi}_b(Q) \\ \bar{\psi}_a(Q) \end{pmatrix} = 0. \quad (\text{C7})$$

The solutions are similar to (C3) and (C5):

$$\bar{\psi}_a(P) = \begin{cases} a_{\text{out}}P^{i|\nu|^2}, & P > 0, \\ a_{\text{in}}|P|^{i|\nu|^2}, & P < 0, \end{cases} \quad (\text{C8})$$

for $P \neq 0$, and

$$\bar{\psi}_b(Q) = \begin{cases} b_{\text{out}}Q^{-i|\nu|^2}, & Q > 0, \\ b_{\text{in}}|Q|^{-i|\nu|^2}, & Q < 0, \end{cases} \quad (\text{C9})$$

for $Q \neq 0$. The relation between the incoming and outgoing amplitudes is given in terms of the \mathbf{S} -matrix relation:

$$\begin{pmatrix} b_{\text{out}} \\ a_{\text{out}} \end{pmatrix} = \begin{pmatrix} \tau & -\bar{\rho} \\ \bar{\rho}^* & \tau \end{pmatrix} \begin{pmatrix} b_{\text{in}} \\ a_{\text{in}} \end{pmatrix}, \quad (\text{C10})$$

where τ is the same as above, while $\bar{\rho} \equiv \rho e^{-2i\theta}$.

APPENDIX D: METAPLECTIC TRANSFORMS

The purpose of this appendix is to present the details of the metaplectic transformations (43)–(44) of (40)–(41), where the generating functions $F_3(p, Q)$ and $F_4(p, P)$ for the canonical transformations (36)–(37) are

$$\begin{aligned} F_3(p, Q) &= \frac{\epsilon}{2} \left(\frac{p^2}{2} + Q^2 \right) - pQ/a_\epsilon, \\ F_4(p, P) &= -\frac{\epsilon}{2} \left(\frac{p^2}{2} + P^2 \right) - pP/b_\epsilon, \end{aligned} \quad (\text{D1})$$

where $(a_+, a_-) = (1, -\sigma)$ and $(b_+, b_-) = (-1, -\sigma)$.

1. Metaplectic transform $\bar{\psi}_j(Q) \rightarrow \psi_j(p)$

For the wave function

$$\bar{\psi}_j(Q) = \begin{cases} z_j^{\text{out}} Q^{-i|\nu|^2}, & Q > 0, \\ z_j^{\text{in}} |Q|^{-i|\nu|^2}, & Q < 0, \end{cases} \quad (\text{D2})$$

the metaplectic transform (43) yields

$$\begin{aligned} \psi_j(p) &= \left(\frac{1}{2\pi i a_\epsilon} \right)^{1/2} \int_0^\infty dQ \\ &\times e^{i\epsilon(p^2/4 + Q^2/2) - i|\nu|^2 \ln Q} (z_j^{\text{out}} e^{-ipQ/a_\epsilon} + z_j^{\text{in}} e^{ipQ/a_\epsilon}). \end{aligned} \quad (\text{D3})$$

Since we are interested in evaluating $\psi_j(p)$ in the large $|p|$ limit, we note that the phase

$$\chi(Q; p) \equiv \frac{\epsilon Q^2}{2} + \frac{\epsilon p^2}{4} - |\nu|^2 \ln Q \mp \frac{pQ}{a_\epsilon} \quad (\text{D4})$$

is a rapidly varying function of Q , except when $\chi'(Q; p) \approx 0$. Denoting $Q_0(p) = \pm(\epsilon p/a_\epsilon - a_\epsilon |\nu|^2/p)$ the point where $\chi'(Q; p)$ vanishes for fixed p (with $|p| \gg 1$), we find that $\chi(Q_0(p); p) \equiv -\epsilon S_\epsilon(p)$. Using the stationary-phase method, we therefore obtain

$$\psi_j(p) = \sqrt{-b_\epsilon} e^{-i\epsilon S_\epsilon(p)} \begin{cases} z_j^{\text{out}}, & \epsilon p/a_\epsilon > 0, \\ z_j^{\text{in}}, & \epsilon p/a_\epsilon < 0. \end{cases} \quad (\text{D5})$$

For $\epsilon = \pm 1$, we obtain (45) and (46) (with the upper sign).

2. Metaplectic transform $\bar{\psi}_j(P) \rightarrow \psi_j(p)$

Similarly, for the wave function

$$\bar{\psi}_j(P) = \begin{cases} z_j^{\text{out}} P^{i|\nu|^2}, & P > 0, \\ z_j^{\text{in}} |P|^{i|\nu|^2}, & P < 0, \end{cases} \quad (\text{D6})$$

the metaplectic transform (44) yields

$$\begin{aligned} \psi_j(p) &= \left(\frac{1}{2\pi i b_\epsilon} \right)^{1/2} \int_0^\infty dP \\ &\times e^{-i\epsilon(p^2/4 + P^2/2) + i|\nu|^2 \ln P} (z_j^{\text{out}} e^{-ipP/b_\epsilon} + z_j^{\text{in}} e^{ipP/b_\epsilon}). \end{aligned} \quad (\text{D7})$$

Since we are interested in evaluating $\psi_j(p)$ in the large $|p|$ limit, we note that the phase

$$\chi(P; p) \equiv \frac{-\epsilon P^2}{2} - \frac{\epsilon p^2}{4} + |\nu|^2 \ln P \mp \frac{pP}{b_\epsilon} \quad (\text{D8})$$

is a rapidly varying function of P , except when $\chi'(P; p) \approx 0$. Denoting $P_0(p) = \mp(\epsilon p/b_\epsilon - b_\epsilon |\nu|^2/p)$ the point where $\chi'(P; p)$ vanishes for fixed p (with $|p| \gg 1$), we find that $\chi(P_0(p); p) \equiv \epsilon S_\epsilon(p)$ and, using the stationary-phase method, we find

$$\psi_j(p) = \sqrt{a_\epsilon} e^{i\epsilon S_\epsilon(p)} \begin{cases} z_j^{\text{out}}, & \epsilon p/b_\epsilon > 0, \\ z_j^{\text{in}}, & \epsilon p/b_\epsilon < 0. \end{cases} \quad (\text{D9})$$

For $\epsilon = \pm 1$, we obtain (45) and (46) (with the lower sign).

¹A. N. Kaufman and L. Friedland, Phys. Lett. A **123**, 387 (1987).

²L. Friedland and A. N. Kaufman, Phys. Fluids **30**, 3050 (1987).

³A. N. Kaufman, "Phase-space plasma-action principles, linear mode conversion, and the generalized Fourier transform," in *Nonlinear and Chaotic Phenomena in Plasmas, Solids, and Fluids*, edited by W. Rozmus and J. A. Tuszynski (World Scientific, Singapore, 1991), p. 160.

⁴A. J. Brizard and A. N. Kaufman, Phys. Rev. Lett. **74**, 4567 (1995).

⁵A. J. Brizard, J. J. Morehead, A. N. Kaufman, and E. R. Tracy, Phys. Rev. Lett. **77**, 1500 (1996).

⁶Y. M. Liang, J. J. Morehead, D. R. Cook, T. Fla, and A. N. Kaufman, Phys. Lett. A **193**, 82 (1994).

⁷A. J. Brizard and A. N. Kaufman, Phys. Plasmas **3**, 64 (1996); Phys. Rev. Lett. **76**, 1639 (1996).

⁸W. H. Press, B. P. Flannery, S. A. Teukolsky, and W. T. Vetterling, *Numerical Recipes* (Cambridge University Press, Cambridge, 1986).

⁹E. R. Tracy and A. N. Kaufman, Phys. Rev. Lett. **64**, 1621 (1990); Phys. Rev. E **48**, 2196 (1993).

¹⁰The dispersion matrices in (38)–(39) have the same dispersion curve: $PQ = |\nu|^2$. A comparison of two ray diagrams indicates that the two conversion types are transformed into each other by a simple labeling $a \leftrightarrow b$ as well as the interchange $\nu \rightarrow \nu^*$. Although physically both types lead to identical transmission and conversion coefficients, the off-diagonal components of their respective \mathbf{S} matrix differ only by a phase factor (see Appendix C).

¹¹W. H. Miller, in *Advances in Chemical Physics*, edited by I. Prigogine and S. A. Rice (Wiley, New York, 1974), Vol. 25, Sec. II.

¹²W. G. Flynn and R. G. Littlejohn, Ann. Phys. **234**, 334 (1994).

¹³H. Goldstein, *Classical Mechanics* (Addison-Wesley, Reading, MA, 1950), Chap. 8.